Computational Design and Optimization of Infrastructure Policy in Water and Agriculture

by

Abdulaziz Alhassan

B.S., King Fahd University of Petroleum and Minerals (2013)

Submitted to the Center for Computational Engineering
in partial fulfillment of the requirements for the degree of

Masters of Science in Computation for Design and Optimization

at the

MASSACHUSETTS INSTITUTE OF TECHNOLOGY

June 2017

Author ..... Signature redacted
Center for Computational Engineering
May 24, 2017

Certified by .... Signature redacted .....
Olivier L. de Weck
Professor of Aeronautics and Astronautics and Engineering Systems
Thesis Supervisor

Certified by. Signature redacted .....
Kenneth Strzepek
Research Scientist, Joint Program and CGCS. Professor Emeritus of Civil, Environmental, and Architectural Engineering, University of Boulder at Colorado
Thesis Supervisor

Accepted by .. Signature redacted .....
Nicolas Hadjiconstantinou
Co-Director, Computation for Design and Optimization

Computational Design and Optimization of Infrastructure Policy in Water and Agriculture

by

Abdulaziz Alhassan

Submitted to the Center for Computational Engineering
on May 24, 2017, in partial fulfillment of the
requirements for the degree of
Masters of Science in Computation for Design and Optimization

Abstract

Investments in infrastructure tend to be associated with high capital costs, creating a necessity for tools to prioritize and evaluate different infrastructure investment options. This thesis provides a survey of computational tools, and their applicability in fine-tuning infrastructure policy levers, prioritizing among different infrastructure investment options and finding optimal sizing parameters to achieve a certain objective. First, we explore the usability of Monti Carlo simulations to project future water demand in Saudi Arabia and then, we use the outcome as an input to a Mixed Integer Linear Program (MILP) that investigates the feasibility of seawater desalination for agricultural irrigation under different water costing schemes. Further, we use numerical simulations of partial differential equations to study the conflicting interests between agricultural and municipal water demands in groundwater aquifer withdrawals and lastly we evaluate the use of Photo Voltaic powered Electro Dialysis Reversal (PV-EDR) as a potential technology to desalinate brackish groundwater through a multidisciplinary system design and optimization approach.

Thesis Supervisor: Olivier L. de Weck
Title: Professor of Aeronautics and Astronautics and Engineering Systems

Thesis Supervisor: Kenneth Strzepek
Title: Research Scientist, Joint Program and CGCS. Professor Emeritus of Civil, Environmental, and Architectural Engineering, University of Boulder at Colorado

Acknowledgments

To my parents, Abdulrahman and Hessa, for their utmost care and encouragement, for always placing their faith in me and pushing me through my endeavors. To my siblings, Mohammed, Riyadh, Faten, Rami, Ziyad, Areej and Ahmed for always being there for me.

To my friends, for providing a network of guidance and companionship when needed the most. My teachers, mentors and professors, to their passion, knowledge and wisdom that enabled me to grow.

To my advisors, Olivier de Weck, who have always provided a unique point of view, and Kenneth Strzepek, a passionate water scientist on a long journey around the world to solve problems and raise awareness, who took me under his wings and made sure I had what it takes to be a better informed water person.

To MIT, and the Center for Computational Engineering, for providing an environment for innovation to thrive. To King Abdulaziz City for Science and Technology for paving my way forward and for their generous scholarship that made this possible. To the Center for Complex Engineering Systems and its co-director, Anas Alfaris for pushing me to the limit.

Thank you.

Contents

List of Figures

List of Tables

Chapter 1

Introduction

1.1 Main Contribution

Investments in infrastructure tend to be associated with high capital costs, creating a necessity for tools to prioritize and evaluate different infrastructure investment options, such as technology use and sizing. While numerical simulations provide a tool to analyze and understand the environment that infrastructure operate in, such as simulating seawater salinity, groundwater flow, storms and dust patterns. Optimization provides a decision tool that could help infrastructure policymakers to investigate many alternatives such as the optimal economic benefit of agriculture, optimal water allocation between competing activities, selecting optimal sizing and technology choice of an infrastructure plant.

This thesis provides a survey of a number of computational tools, and their applicability in fine-tuning infrastructure policy levers, prioritizing among different infrastructure investment options and finding optimal sizing parameters to achieve a certain objective.

The Second Chapter assesses the water balance in Saudi Arabia, and explores the usability of Monti Carlo simulations to project future water demand in Saudi Arabia on a regional level for both municipal demand and agricultural demand. For each demand category, three demand scenarios are picked as expected high, medium and low scenarios, then are matched to three supply scenarios varying in their supply

source composition.

The Third Chapter starts off with an investigation of agricultural economics and history in Saudi Arabia, and looks at the food balance in the country. A spatial representation of agriculture in the country is constructed. That spacial representation together with the agricultural demand forecasts constructed in Chapter Two are used as inputs to a Mixed Integer Linear Program (MILP), an optimization tool that investigate the feasibility of seawater desalination for agricultural irrigation. Later, a set of alternative water pricing schemes are constructed that are driven by willingness to pump groundwater, willingness to desalinate seawater and the cost of virtual water imports. Those water pricing schemes are compared to the current municipal water tariff in Saudi Arabia.

In Chapter Four, a numerical simulation of the groundwater partial differential equation is developed, using a finite difference scheme to study the conflicting interests between agricultural and municipal water demands in groundwater aquifer withdrawals around the city of Riyadh, Saudi Arabia. The accuracy of that simulation is analyzed, and then provide an assumption biased quantification of the hydraulic head change with and without agricultural activity around the city.

Chapter Five analyzes the use of Photo Voltaic powered Electro Dialysis Reversal (PV-EDR) as a potential technology to desalinate brackish groundwater for municipal use in Saudi Arabia through a multidisciplinary system design and optimization approach. The chapter begins by defining a model and its submodules, and then constructing a set of objective functions. A full factorial design space exploration is used, and then optimal solutions are found through gradient based and heuristic based methods. multiple objectives are handled through a manual weighted sum method and a full factorial study. Outcomes are compared in both the gradient-based optimization and the heuristic based optimization.

1.2 Planning, Policymaking, and Reforms in Saudi Arabia

Saudi Arabia issued it's first "Development Plan" in 1970. That plan aimed to achieve economic diversification away from oil exportation as its first priority. The 10th Plan was released in 2015 and had similar goals to the first few ones. Particularly, the diversification goal was in every development plan ever issued in the 45 years between 1970 and 2015, but the government's income base has been dominated by oil rents. The collapse of oil prices in the end of 2014, and the sustained low prices that followed, prompted the government to exercise many austerity measures: including reductions in capital investments, freeze in government workers raises and slashes in benefits, phasing out many government subsidies in the water and energy sectors, and (for the first time in its history) imposing a value added tax (VAT). Those policy reforms were rolled out as part of the Fiscal Balance Program announced in 2016, which aims to eliminate government deficit that resulted from the 2014 decline in oil prices. This Fiscal Balance Program is one of a set of programs under the "Vision 2030", an overarching framework meaning to achieve the historic goal of weaning the Saudi Arabian economy away from dependence on oil rents, with minimal socioeconomic disruption.

New policy reforms under "Vision 2030" share a few basic objectives: spending rationalization, efficiency increases and subsidy cuts. one can argue that the analysis provided in this thesis can provide a starting point for a policy-driven, optimality oriented, efficient water infrastructure planning toolkit. This work is intended to serve as a survey for a set of tools and their applicability to decision making and infrastructure policy agenda setting. The conclusions discussed henceforth are dependent on the specific spatio-temporal context and should only be taken as a pre-feasibility analysis. Further, location specific, context specific analysis is needed to enable decision making on a refined level.

Chapter 2

Modeling Saudi Arabia's Water Resources

2.1 Water Resources in Saudi Arabia

Saudi Arabia, although energy rich, is poor in its water resources. The country is part of an arid region where there is no access to any form of fresh surface water. Saudi Arabia resorted to the energy intensive seawater desalination for municipal use to supplement groundwater resources that are being strained by agricultural activity, raising the need to study the country's water-energy-food nexus. This chapter uses population and agricultural trends to build futuristic water demand scenarios, and proposes a set of variations on population growth and agricultural policy. This chapter matches demand scenarios with supply scenarios. Exploring the effect of these variations, estimates the possible ranges of resources needed, either as groundwater withdrawals or as energy requirements for desalination. This enables decision makers to make better-informed sustainable decisions. A specific policy on seawater desalination for agriculture is thoroughly investigated.

Saudi Arabia is divided into 13 administrative regions; each region has a capital that is usually the largest city in that region. In 2010, the population of Saudi Arabia was 27 million, 65% of the population lived in the three major regions of Saudi Arabia: Makkah, Riyadh and the Eastern Region [1]. This chapter will look into the water

balance of Saudi Arabia on the regional level.

The scarcity of rainfall in Saudi Arabia led to the absence of any permanent sources of surface water, forcing Saudi Arabia to rely on two main sources to satisfy water demand: ground water aquifers and seawater desalination. Presently, agricultural demand depends completely on ground water, while industrial and municipal demand are met through a combination of groundwater extraction and seawater desalination [2].

Groundwater in Saudi Arabia can be described as fossil water. Due to limited rainfall and excessive consumption, the major groundwater aquifers are being depleted. A study estimated the storage of the main and secondary aquifers in 1984 to be around 500 billion cubic meters and a study in 1996 estimated the amount to be 289.1 billion cubic meters [4]. Taking into consideration the reported consumption rates since then, the state of groundwater resources in Saudi Arabia is unsustainable [5], and measures should be taken from either demand or supply side (or both) to put the state of water resources in a more sustainable path.

The state of the groundwater is based on limited available data with a large degree of uncertainty. This is due to the fact that estimating exact figures of ground water levels is a difficult and uncertain task. We could end up either overestimating or underestimating ground water levels with a significant margin of error. More studies are needed to better evaluate the current state of ground water levels to make plans that are more reliable for the future. In addition, it is unclear if we are constrained by extraction rates. It's uncertain that Saudi Arabia could reach a point in which possible extraction rates could be a limiting factor to supply.

Excessive extraction of groundwater is associated with increased financial costs. Lower groundwater levels would add more energy demand for extraction from deeper wells. Deeper wells cost more to be dug, and water quality degrades significantly with excessive groundwater withdrawal [4, 6].

This study proposes regional scenarios where alternatives in major demand drivers are used, and matched with proposed supply scenarios, The scenarios are applied to Saudi Arabia as a case study.

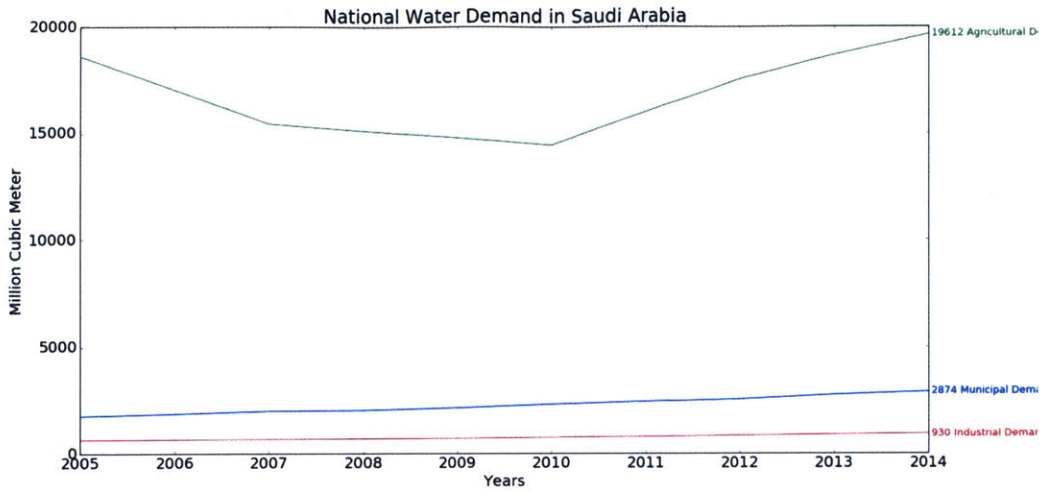

Figure 2-1: Historical Agricultural, Industrial and Municipal water demand [2]

2.2 Overview of Water Supply and Demand In Saudi Arabia

We can see from Figure 2-1 that agricultural water demand constitutes 83% of the total water demand in Saudi Arabia in 2014. The remaining 17% is municipal and industrial water demand [2]. Agricultural water supplies are coming from the fossil ground water reserves. The only water costs that farmers bare is the cost of energy needed to pump water from the ground up, and they usually rely on energy resources that are heavily subsidized by the Saudi government [5]. This makes water costs marginal and there is no incentive for farmers to invest in water efficient irrigation systems.

Municipal water demand is dependent on seawater desalination (Figure 2-2). Fifty-six percent of municipal water supplies come from desalination plants that are located on both the east and west coasts of Saudi Arabia [2]. Desalinating seawater is an energy intensive process. The energy requirements of those desalination plants are supplied from Saudi Arabia's oil and gas reserves, and utility companies purchases of fuel are heavily subsidized.

2.3 Demand Projection Methodology

To project demand, a driver-intensity approach is used, where different demand categories are associated with drivers (Population, agricultural land ares,...) and intensities (Per capita consumption, crop water requirements, ...). A Monte Carlo process is used to project the future values of those drivers and indicators with a confidence interval, and then the value of a driver is multiplied by the value of an indicator to come up with an estimate projection for future water demand across different categories.

The Monte Carlo process looks at historical values of either a driver or an indicator, then it builds a probability distribution of historical growth rate percentages. Then the process generates a number of random walks that draw from the constructed random distribution. The 90th percentile, mean and the 10th percentile for those random walks are used as the high, medium and low scenarios respectively. The random walk is constrained by a growth rate limit, and has a diminishing factor that declines with time. This Monte Carlo process is parameterized by the following parameters;

- Last simulation year
- Number of random walks
- Bound on growth rates
- The diminishing factor

And the demand projection is obtained through the following formula:

$$M_p^y = (1 + U(min(D_g), max(D_g)))D_{y-1}(1 + U(min(I_g), max(I_g)))I_{y-1}$$

Where:

- M_p^y: is demand projection at year y
- D_y Driver value at year y

- I_y Intensity value at year y
- $U(min(D_g), max(D_g))$: a random variable drawn from a uniform distribution bounded by the minimum and maximum historical driver growth rate

Using this formula to generate multiple random walks that project future demand through indicators and drivers, we define three demand projections:

- **High** the ninetieth percentile of all generated demand random walks
- **Medium** the mean of all generated demand random walks
- **Low** the tenth percentile of all generated demand random walks

2.4 Municipal Water Demand

2.4.1 Background

Municipal water demand in Saudi Arabia is driven by population growth. Population in Saudi Arabia grew significantly in the 1970's and 1980's with growth rates touching 6.5% due to the jump of quality of life that was associated with the government's oil income. The period of the 1990's and the 2000's exhibited a slower population growth rates with a growth rate of around 2% in 2013 [7].

The last two official censuses (2004, 2010) show varying growth rates across regions. This can be attributed to the fact that some regions are more economically mature than others; causing inter-regional migration towards the more economically developed regions.

Table 2.1 shows the variation of population demand across regions. Regions vary in their water supply source. Desalination constituted 58.4% of municipal water supplies. Ninety-nine percent of municipal water supplies in Makkah region came from seawater desalination, where Hail, Northern Borders, Najran, Baha and Jawf regions relied completely on groundwater. Table 2.1 shows variation of the contribution of desalination across all regions. We can see from Figure 2-2 that the contribution of desalination is following an increasing trend.

Table 2.1: Variations of population, growth, demand and per capita municipal demand [2, 8]

Region	Population (2013)	Population Growth Rate (2004 -2010)	Municipal Demand (2013, MCM per Year)	Municipal Demand Growth Rate (2006-2013)	Contribution of Desalination (2013, %)	Per Capita consumption (2013, M^3 per Person)
Saudi Arabia	30387506	3.3	2731	5.7	58	90
Riyadh	7733415	3.9	808	4.6	41	105
Makkah	7736211	3.3	676	9.7	99	87
Madinah	1972818	3.0	178	4.6	85	90
Qassim	1360856	3.3	120	0.7	3	88
Eastern Region	4645516	3.7	599	2.9	55	129
Asir	2083276	2.4	76	8.2	89	36
Tabuk	865861	2.5	99	12.2	10	114
Hail	650172	2.4	32	3.5	0	50
Northern Borders	350702	2.5	23	15.7	0	65
Jazan	1496944	2.6	38	14.5	65	26
Najran	567288	3.4	24	14.5	0	42
Baha	439697	1.7	16	14.4	0	37
Jawf	496401	3.6	40	2.6	0	81

Per capita demand is also varying across regions. Figure 2-3 shows that the Eastern Region is the highest with 129 cubic meter per person per year in 2013, while Jazan's per capita consumption was the lowest at 26 cubic meter per capita per year.

Municipal demand can be characterized to be seasonally fluctuating, demand rises during summer months, and maximal monthly demand usually falls around July. Demand falls during winter, reaching minimal monthly demand around February. Figure 2-4 shows seasonality. The proportion of maximum monthly demand to minimum monthly demand averaged 1.243:1 and the fluctuation of demand is mapped to fluctuation in both supply sources. The proportion of maximum monthly supply to minimum monthly supply averaged 1.239:1 and 1.265:1 for ground water supply and

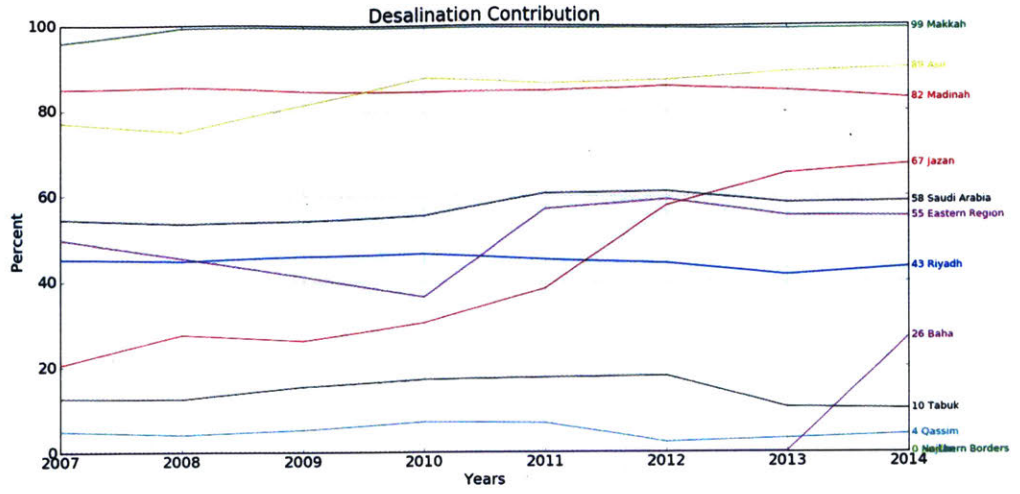

Figure 2-2: Historical desalination contribution to municipal demand, by region [9]

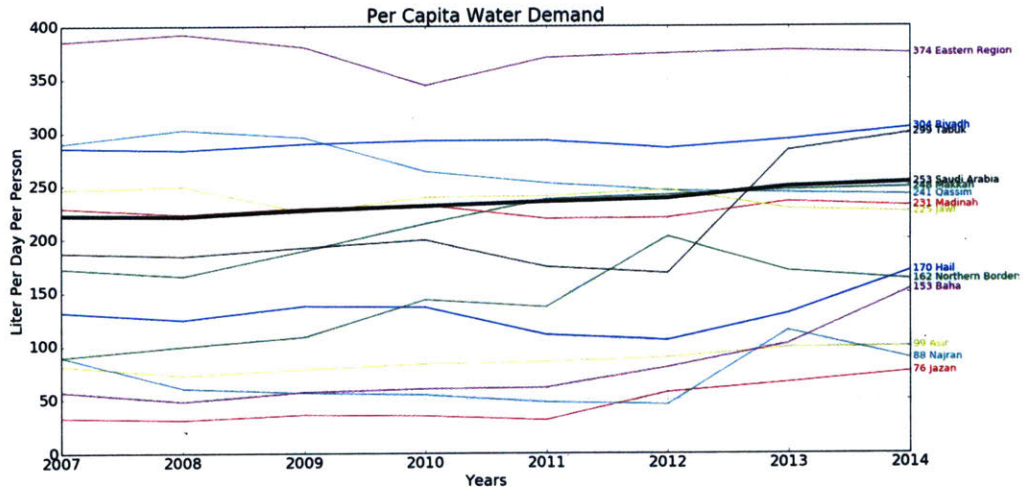

Figure 2-3: Historical municipal demand per capita [9]

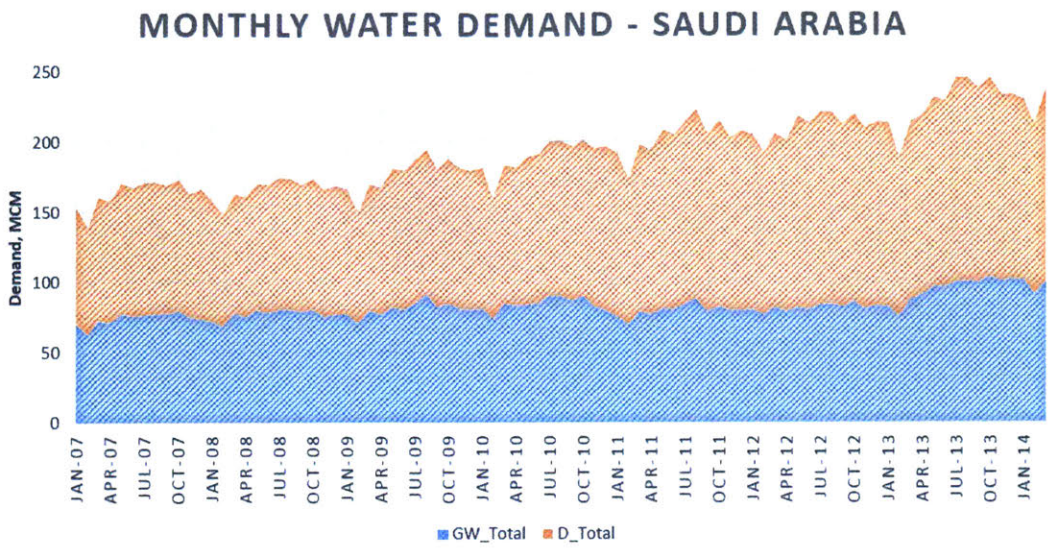

Figure 2-4: Historical municipal water demand showing seasonality and contribution of groundwater and desalination, national [9]

desalinated water supply respectively [9].

2.4.2 Municipal Demand Projections

Following the earlier described Monte Carlo demand projection methodology, municipal demand is associated with population as a driver, and with per capita consumption as an intensity. A Monte Carlo process is used for each of the thirteen regions, for both the driver and intensities. Figure 2-5 shows three scenarios for per capita consumption, and Figure 2-6 shows three scenarios for population. A municipal water demand projection is then generated (Figure 2-7). The latest available data year shows that municipal demand across Saudi Arabia stands at 2,874 MCM in 2014. The high, medium and low scenarios project municipal demand to reach 5,000; 6,500; 8,000 MCM respectively of municipal demand in Saudi Arabia in 2035.

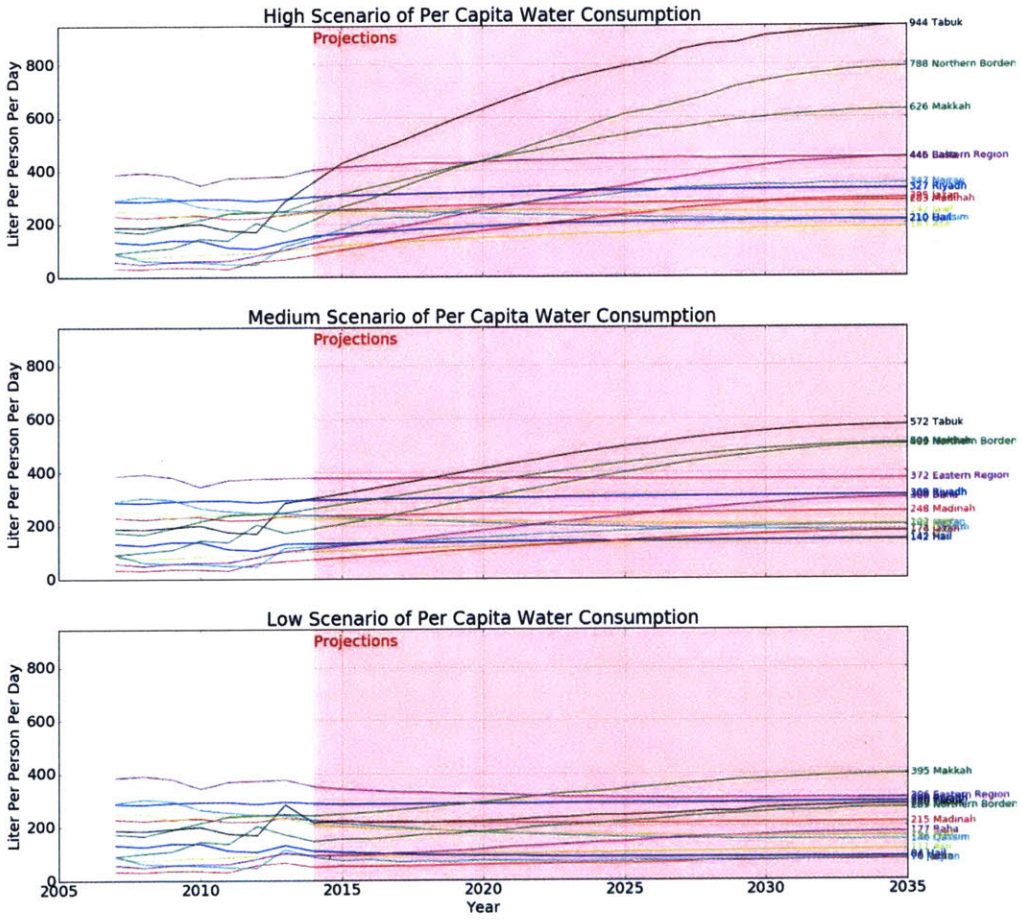

Figure 2-5: Three scenarios for per capita water demand projections

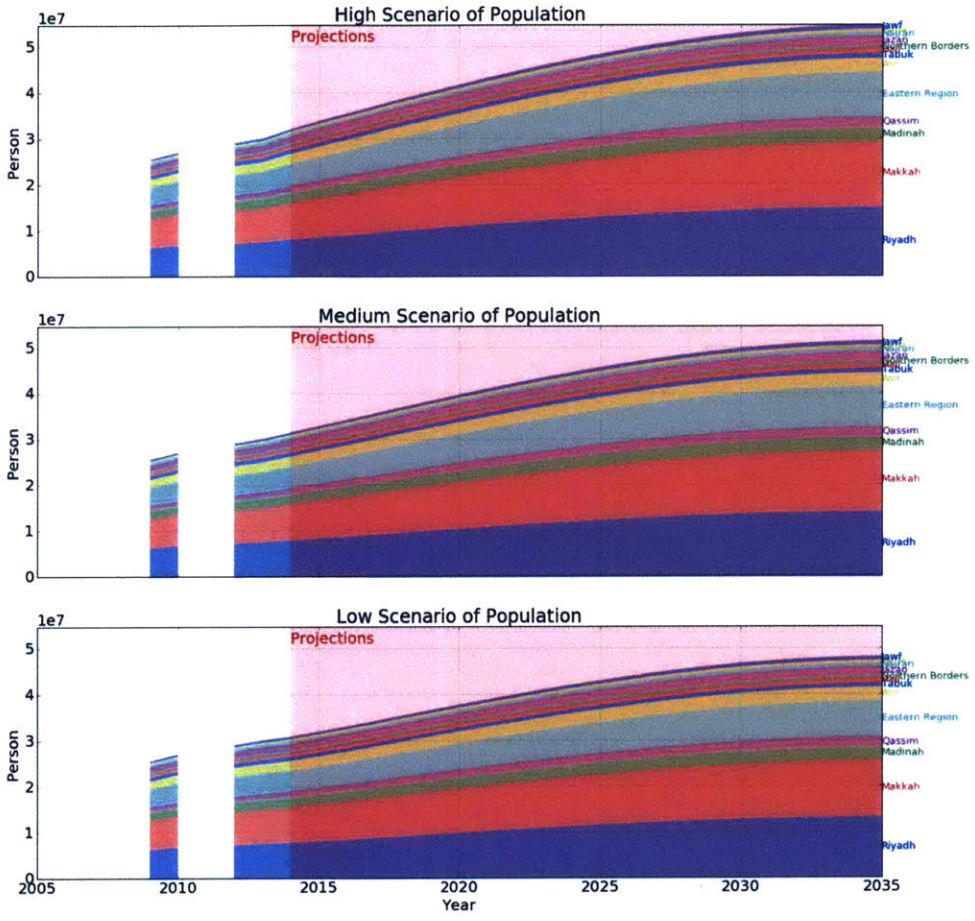

Figure 2-6: Three scenarios for Population projections

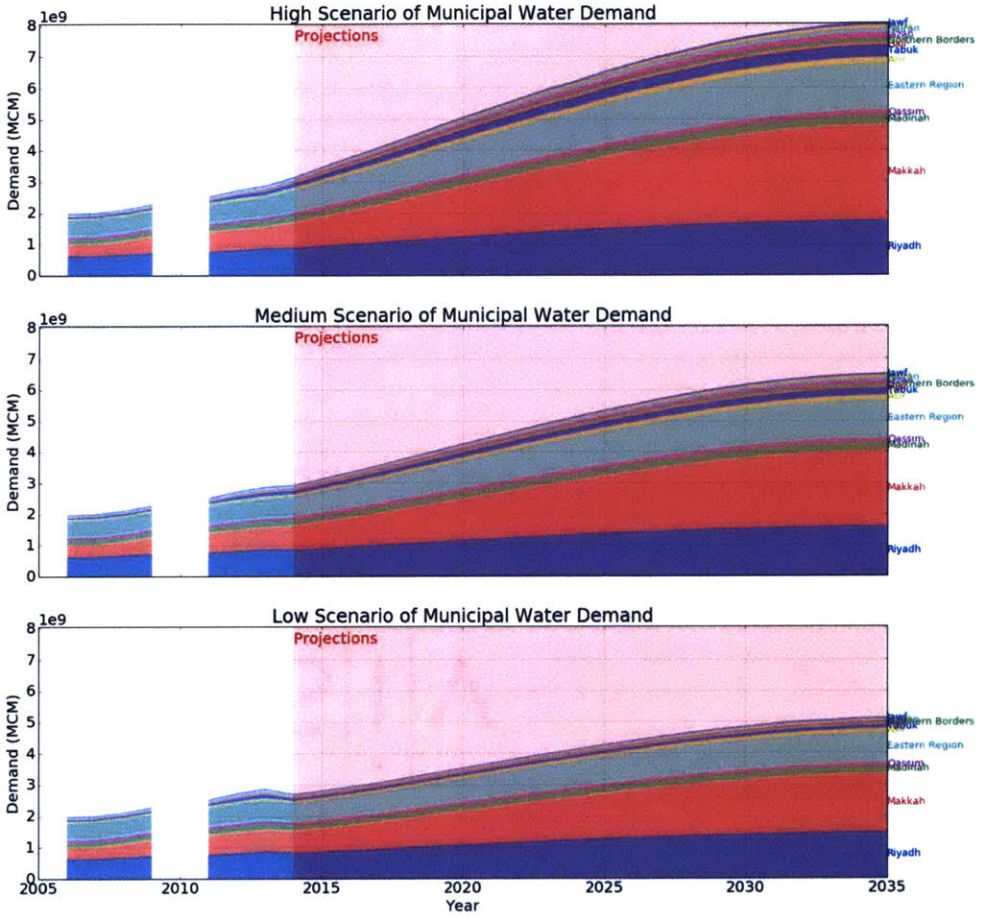

Figure 2-7: Three scenarios for municipal water demand projections, obtained by using population as a driver, and per capita water consumption as an indicator

2.5 Agricultural Water Demand

2.5.1 Background

Agricultural water demand in Saudi Arabia is investigated as it historically constituted the largest bulk of national water demand. in order to build projections, the same driver-intensity approach is followed, where agricultural land areas are used as drivers, and per unit of area water requirements as intensities. As those intensities vary across geographical locations and types of crops, The analysis is broken down into four families of crops:

- **Vegetables**: tomatoes, cucumbers, ...etc.
- **Cereals**: wheat, malt, ...etc.
- **Fruits**: Dates, grapes, ...etc.
- **Fodder**: Barley, alfalfa, ...etc.

The intensities (per area water requirements) used in this analysis are based off of the ones generated in [16]

2.5.2 Agricultural Water Demand Projection

From Figure 2-8, the following is observed about each of the four crop families

- **Vegetables**: In the near history, vegetable growing in Saudi Arabia has been stable, as it wasn't directly impacted by a policy control. The High scenario shows a slight increase in land areas dedicated to vegetable growing, while the Medium and Low scenarios showed a slow, minor, gradual decline in areas dedicated to grow vegetables.
- **Cereals**: as a result of a recent policy changes (Discussed in details in Chapter 3), and due to the recent inclination to import cereals as opposed to growing them locally in Saudi Arabia, we see a steady decline in the area dedicated to

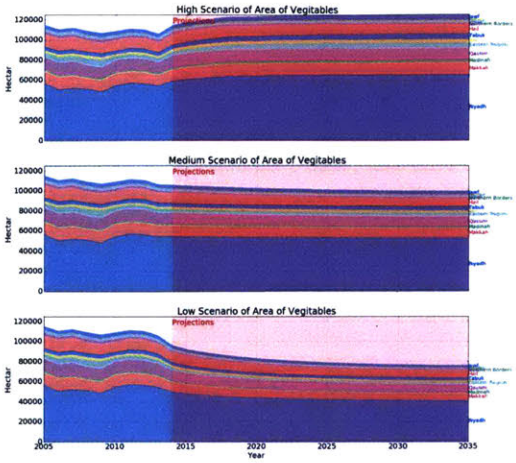

(a) Projections of Areas of Vegetables

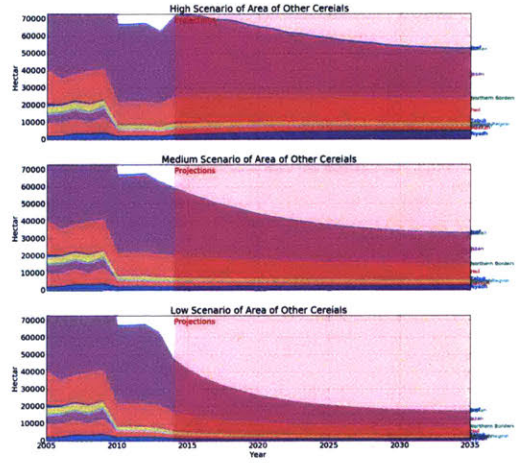

(b) Projections of Areas of Cereals

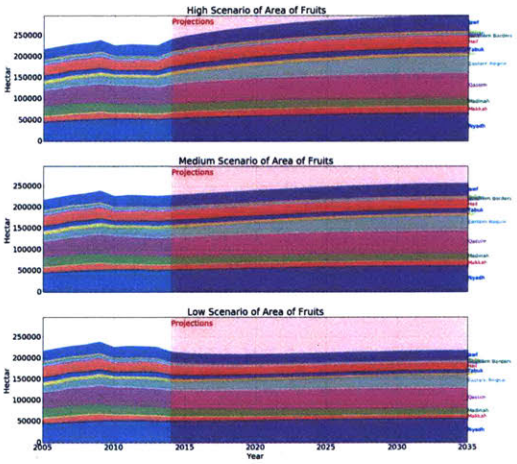

(c) Projections of Areas of Fruits

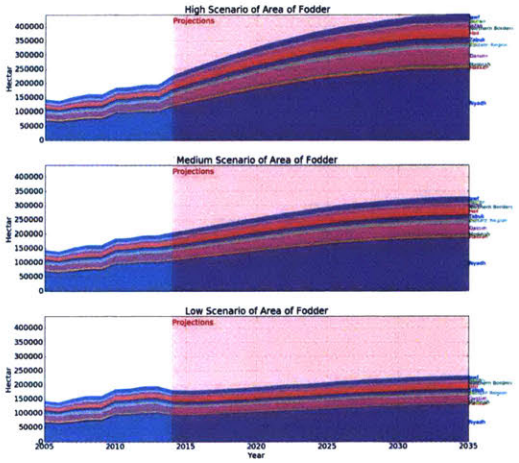

(d) Projections of Areas of Fodder

Figure 2-8: Three scenarios for Crop land areas across the four crop families

growing cereals across the three scenarios, with the High scenario exhibiting a slow decline, while the Medium and Low showing a steady and sharp declines respectively.

- **Fruits**: Similar to the dynamics in vegetables, the land dedicated to grow fruits is expected to grow in the High and Medium scenarios, while the low scenario showed a minor decline.

- **Fodder**: it is interesting to observe that the area dedicated to grow fodder has increased across the three scenarios. This can be attributed to a recent change in policy (more details in Chapter 3), where a restriction on growing wheat led farmers to grow fodder instead, as it uses the same infrastructure, while it constitute an economically vital crop to farmers, and a good substitute for the no longer subsidized wheat. While the Low scenario showed only a slight increase, the Medium and High scenarios showed an increase of around 50% and 100% in Fodder land areas respectively.

Using those projections in land areas dedicated to different families of crops as drivers to agricultural water demand, and using the geographically varying crop family water requirements generated in [16] as intensities, three demand projections are constructed. Shown in Figure 2-9, the high scenario proposes a doubling in agricultural water demand by 2035 from its levels in 2013, while the Medium scenario projects an increase of 50% and the low scenario expects a minor increase. The variation between the three scenarios is mainly a result of the variation of the amount of land dedicated to growing fodder. A key message of this analysis is that policies centered around growing fodder would play a pivotal role in any proposed agricultural water demand reduction scheme.

2.6 Water Supplies in Saudi Arabia

While Agricultural demand is met completely by groundwater, municipal demand is met via a combination of groundwater and seawater desalination. Based on the mu-

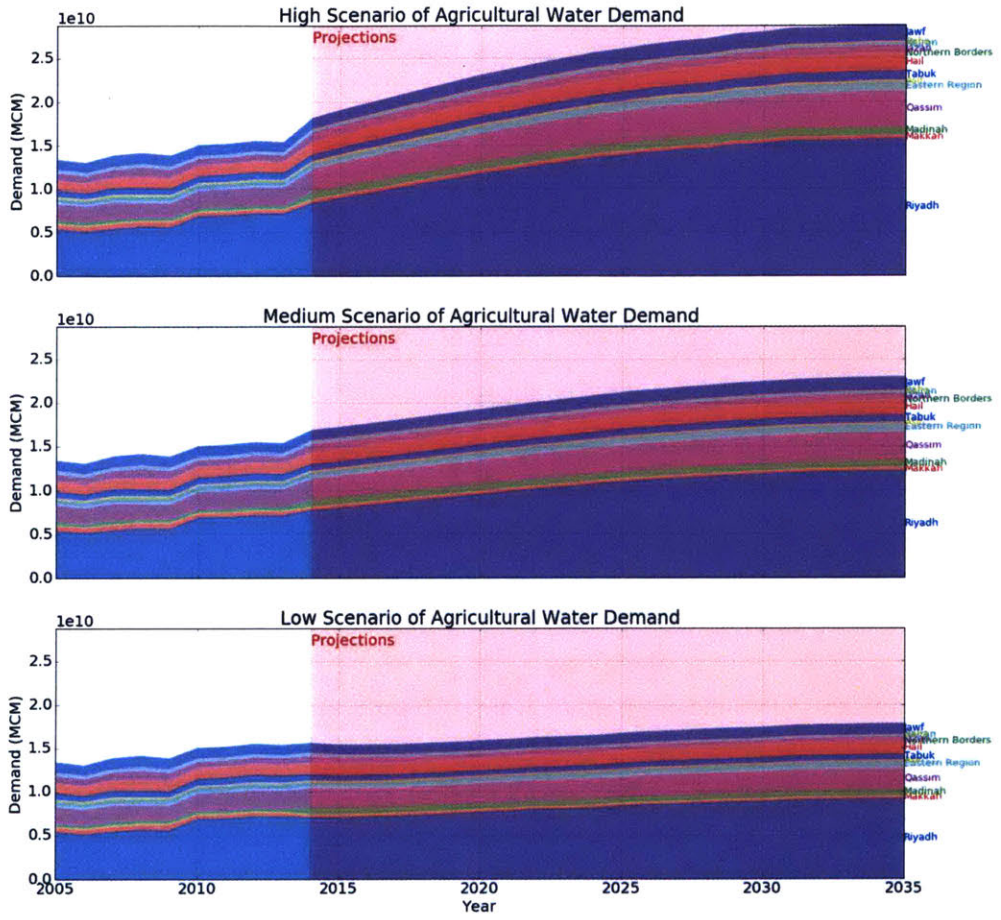

Figure 2-9: Three scenarios for agricultural water demand projections, obtained by using crop family land area as a driver, and per area water requirement as an indicator

nicipal demand projections in section 2.4.2, we propose three scenarios on desalination contribution to municipal demand:

1. **Constant Capacity:** Where no further expansion of the existing desalination infrastructure is assumed, and that 2013 desalination capacity would remain fixed.

2. **Constant Contribution:** Where desalination contribution percentage is assumed to remain fixed at its 2013 levels. Desalination capacity would grow to cover the same percentage that it was covering in each region.

3. **Growing Desalination:** Where desalination would supply hundred percent of demand in coastal regions (Makkah, Madinah, Eastern Region, Asir, Tabuk and Jazan) in addition to Riyadh region, which already receives majority of its supplies from seawater desalination.

Figure 2-10 shows the total supply requirements in the period from 2010 to 2050 for all the combinations of the following scenarios:

- Municipal Demand Scenarios (High, Medium and Low)

- Agricultural Scenarios (High, Medium and Low)

- Desalination Scenarios (Constant Capacity, Constant Contribution and Growing Capacity)

The amount of groundwater withdrawals over the period ranged between 290 billion cubic meters and 1030 billion cubic meters. The variation is mainly related to the agricultural scenario component. Seawater desalination requirements for the period of 2010 to 2050 are estimated to vary between 65 billion cubic meter and 141 billion cubic meters. This variation is linked to both variations in the population scenarios and desalination scenarios.

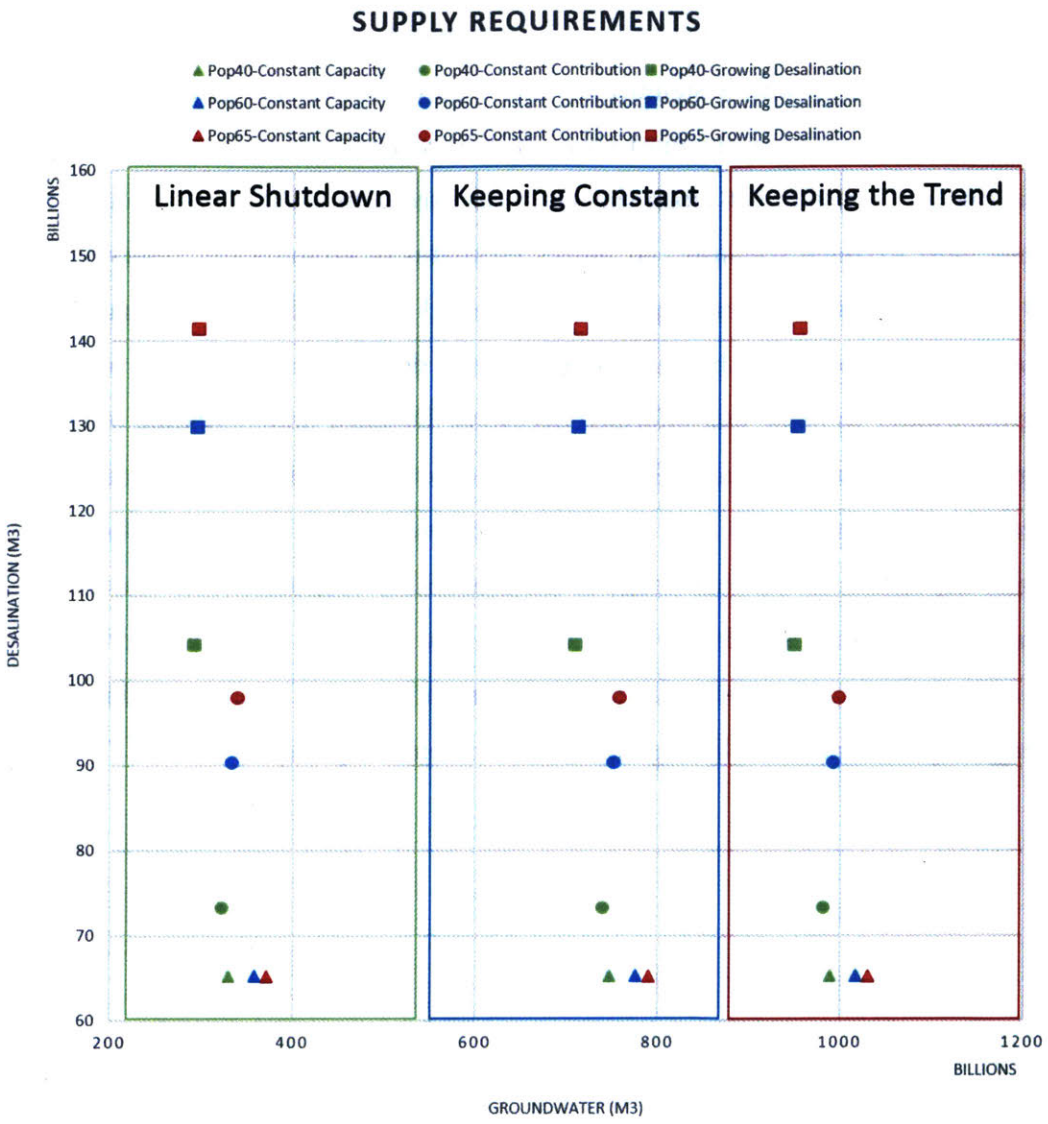

Figure 2-10: Supply requirements of the 27 scenario combinations

2.7 Conclusion

In this chapter, a scenario based regional water supply and demand model is described, in which three scenarios on population as a driver for municipal use, and three scenarios on agricultural land area as a driver for agricultural demand are proposed and three scenarios on supply breakdown are introduced. The impact of agriculture on groundwater withdrawals is significant. The need to extract 290 Billion cubic meters of groundwater needed in the most conservative scenario over the period of 2010-2035 is significant by itself. Let alone the worst-case scenario of 1030 billion cubic meter in the most extreme scenario. [4] Shows estimates of groundwater reserves of only 289 Billion in 1996, but consumption in the period of 1996-2013 proved that estimate wrong. It is obvious that there is a need for more detailed understanding of the state of groundwater to make well-informed decisions. Detailed understanding of the state of ground water would enable Saudi Arabia to better plan its seawater desalination infrastructure, where and how large the next desalination investment should be is totally dependent on our knowledge of the availability of groundwater resources. Demand side measures should be taken as well, the excessive groundwater withdraws for agriculture would lower groundwater levels and degrade quality, leading to more energy requirements to deliver groundwater to demand points.

Chapter 3

Saudi Arabia's Agriculture Policy

3.1 Background

Up until the oil boom in the nineteen seventies, agriculture in Saudi Arabia was limited to smaller scale, family owned and operated farms that relied on manual labor and animal operated shallow groundwater wells that are highly susceptible to drought and fluctuations in rainfall that influence recharge rates. The economic boom in the nineteen seventies enabled the Saudi Arabian government to incentivize and subsidize the development of agriculture as part of a larger effort to increase economic diversification. The sector, through government land grants and interest-free loans, became less labor intense, more mechanized [11]. Animal operated shallow wells were replaced by electricity and diesel driven pumps enabling access to deep, fossil water aquifers that are more reliable and less exposed to seasonal variations. Those fossil, deep aquifers wells offered a consistent and reliable source of water that enabled smaller family farms to grow, and opened the door to large-scale corporation farming business. This growth in deep aquifer water extraction resulted in increased demand in energy for agricultural use, and also led to a swift decline in groundwater tables in many of the main aquifer systems.

One of the goals of developing the agricultural sector is to achieve food security. At some point, Saudi Arabia exceeded the point of self-sufficiency and started exporting wheat. The government acknowledged the severe consequences of the unbound

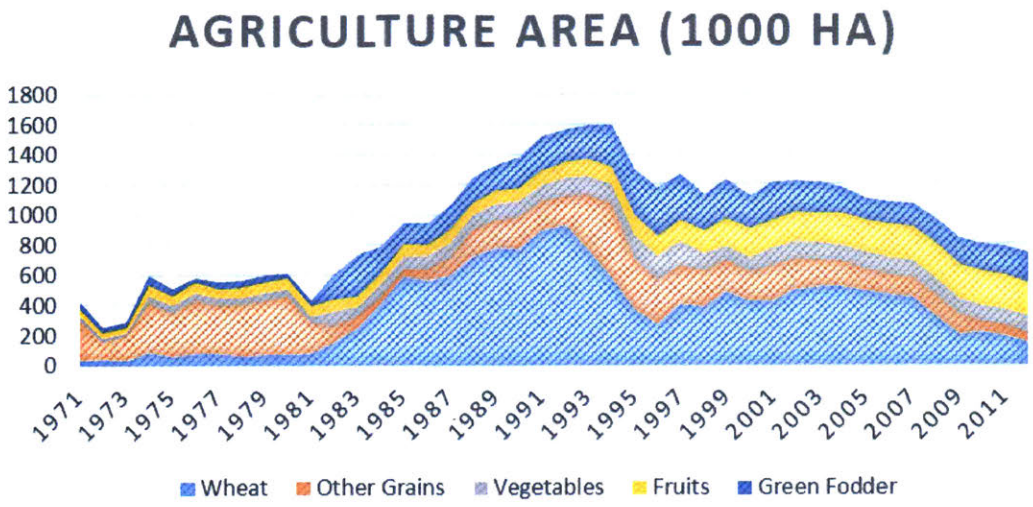

Figure 3-1: Historical agricultural land area showing major crop families, national [10]

expansion in agriculture on the limited water resources; fossil water being the sole supplier of water for agricultural activity is being depleted in faster rates than what was accounted for. In the mid 2000's, the government started regulating agriculture, limiting the number of new water well permits, banning the exportation of fodder, stopping permits to grow fodder, and shutting down its wheat purchasing program in an eight year process, reducing its purchases by 12.5% annually to stop purchasing wheat in 2015 [11].

3.1.1 Economic Implications of Agriculture

Modern agriculture was incentivized by the government as a way to diversify the economy away form oil extraction, This effort led to the growth of agricultural land area (Figure 3-1) from around 400 thousand hectares in 1970 to peak at around 1,600 thousand hectares in the mid 1990's. Since then, agricultural land area has been in a declining trend [10].

In constant 2010 Saudi Arabian Riyals (SAR), the agricultural GDP rose from 5 billion SAR in 1970 to more than 40 billion SAR in 2012. Agriculture contribution to GDP (Figure 3-2) peaked at above 6% in the late 80's and 90's. Agriculture

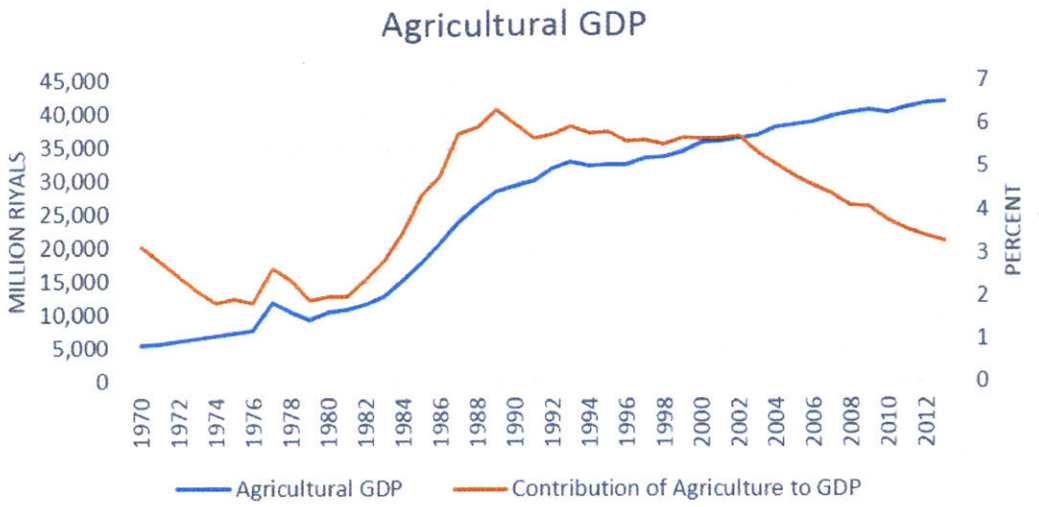

Figure 3-2: Agricultural GDP, and contribution of agriculture to overall GDP, national [10]

contribution declined steadily in the 2000's until it reached 3% in 2012 [11]. The steady decline in agriculture's share of GDP is attributed to the higher growth of other components of GDP.

The agricultural sector accounted for 339,000 jobs in 1999, constituting 6.1% of jobs in the economy, the number of jobs grew to 515,000 jobs in 2012, but the overall number of jobs in the economy grew at a faster rate, reducing the share of the agricultural sector to 4.9% of all jobs in the labor market [12]. Labor productivity, measured in Saudi Riyals per worker in agriculture is the smallest across all sectors shown in Figure 3-3. While GDP productivity in agriculture was only 0.08 million SAR per worker, it was 0.13 in retail and 7.2 in oil and mining. Similarly, agriculture ranks last in terms of labor compensation across sectors shown in Figure 3-4, measured by Saudi Riyals per worker, agriculture only paid 8,600 Annualy, compared to 22,400 in retail and 200,300 in oil and mining.

3.1.2 Food Imports

In 2012, Saudi Arabia produced slightly less than 10 million tonnes of locally grown agricultural crops [18]. This amount has been fairly stable through the past decade.

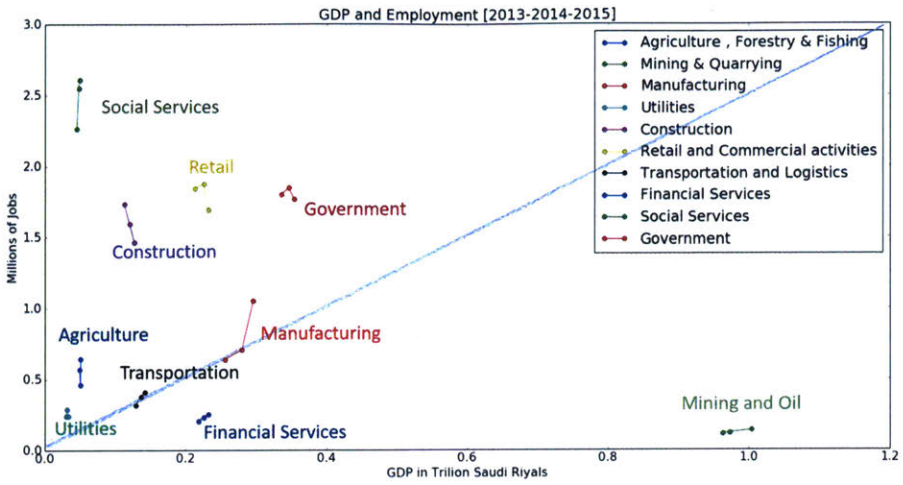

Figure 3-3: Comparing 10 economic sectors of the economy in terms of GDP and Employment

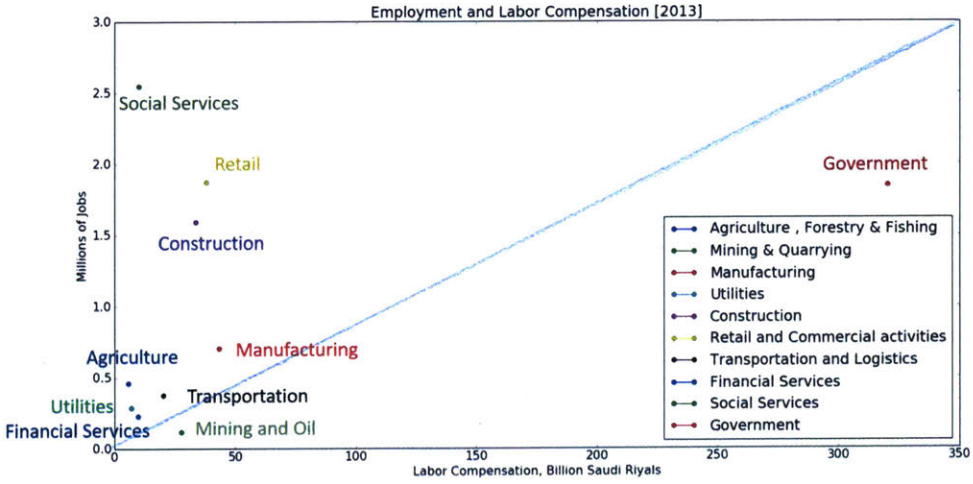

Figure 3-4: Comparing 10 economic sectors of the economy in terms of Employment and Labor Compensation

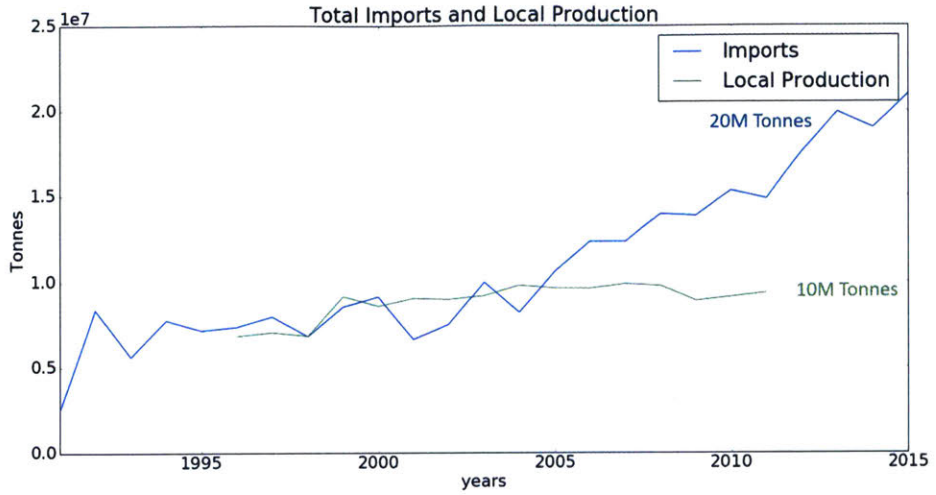

Figure 3-5: Saudi Arabia's local production of food, and food imports [18]

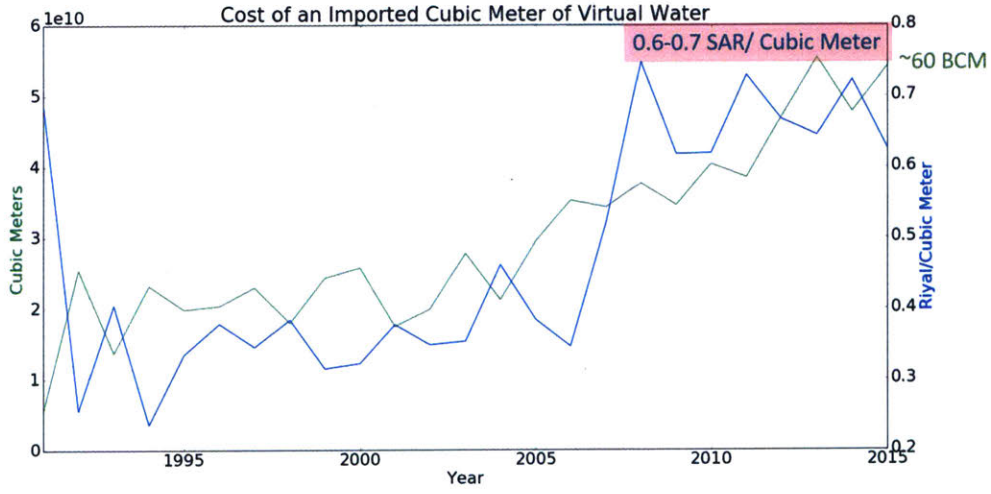

Figure 3-6: Estimates of Saudi Arabia's virtual water imports, and the price per cubic meter of virtual water imported.

Increased demand on agricultural crops has been mainly met by increasing crop imports, where the amount of imported crops has doubled from 10 million tonnes in 2005 into 20 million tonnes in 2015 (Figure 3-5).

We can look at Saudi Arabia's imports of agricultural crops as importing virtual water, we estimate that Saudi Arabia in 2015 imported around 60 billion cubic meters of virtual water; this is based on the assumption that imports carry water that would be needed to grow those crop imports locally. Saudi Arabia, in 2015, spent 35 billion Saudi Riyals on its crop imports (Figure 3-6).

3.2 Spatial Distribution of Agricultural Groundwater Withdrawals

We use the Global Map of Irrigation Areas (GMIA) [17] that was produced by the Food and Agriculture Organization (FAO). The GMIA maps are produced through an algorithm that uses Landsat satellite imagery, MODIS Vegetation Indices and several large-scale irrigation maps to come up with the global spatial distribution of irrigated areas. The map resolution is a 0.25 by 0.25 degrees and each cell shows the intensity of irrigated agriculture in each location.

The Saudi Arabian Ministry of Agriculture publishes an annual statistical book that shows estimates of production in tons, and land areas in hectare for the main crop families (Cereal,Fodder, Fruit and Vegetables). Those estimates are on a regional level. We took those regional estimates, and we assume a uniform distribution of crop types across the same region to come up with a specially distributed map of crop location using the GMIA database.

We use estimates on crop water footprint that take into account regional variations in irrigation systems, climate effects and differences in the composition of each crop family to come up with estimates for regional estimates of crop water footprint [3]. Combining the spatial distribution of irrigated areas from GMIA, estimates of crop land areas from MOA with the regional estimates of crop family water footprint, we

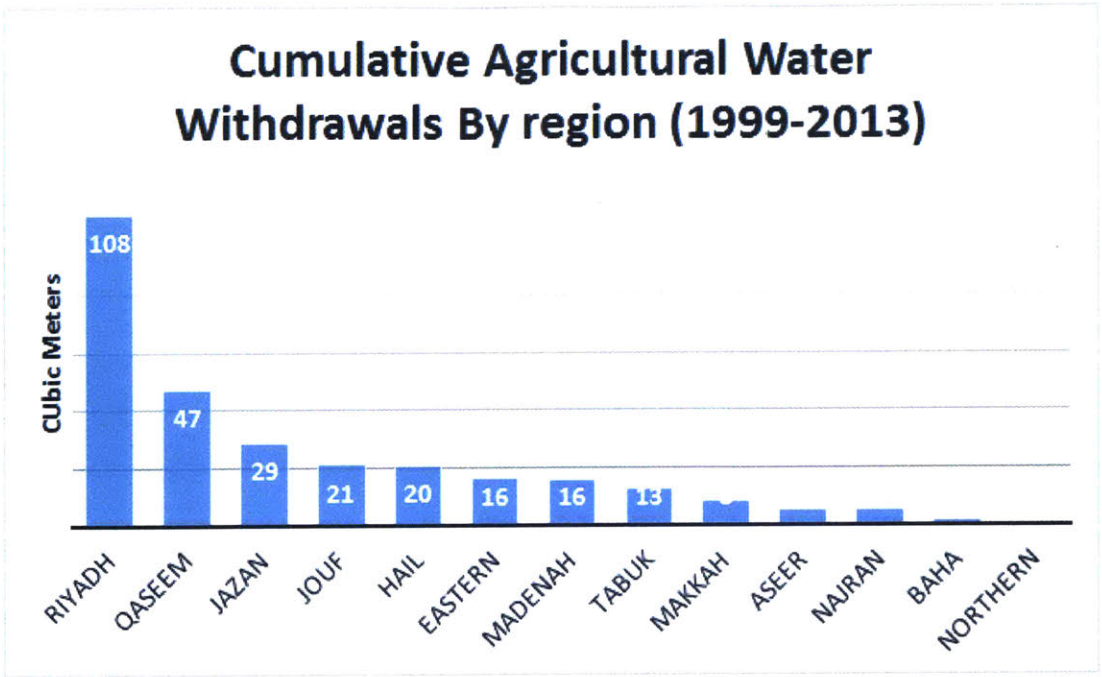

Figure 3-7: Cumulative agricultural water withdrawals across 13 regions between 1999 and 2013

generate a map (Figure 3-7) of the spatial distribution of the amount of water used in agricultural activity. Between 1998 and 2013, it is estimated that there was around 290 billion cubic meter (BCM) of water that was consumed in the agricultural sector (Figure 3-8). Consumption in Riyadh was 108 BCM, 47 in Qassem, 21 in Jouf and 20 in Hail. Those regions constitute the central spine of agricultural activities, and all are inland regions, with no sea access and extremely low levels of precipitation. Those regions are fully reliant on groundwater for all agricultural activity.

3.3 The Energy Footprint for Water in Agriculture

The energy footprint of agricultural activity results from the energy required to pump groundwater from deep aquifers to the surface. Energy pumping costs depends on the amount of water withdrawn, the depth of the well and the per volume unit energy costs. In section 3.2, the amount of water withdrawn for agricultural purposes between 1999 and 2013 is estimated to be at 290 BCM. There is limited available data that

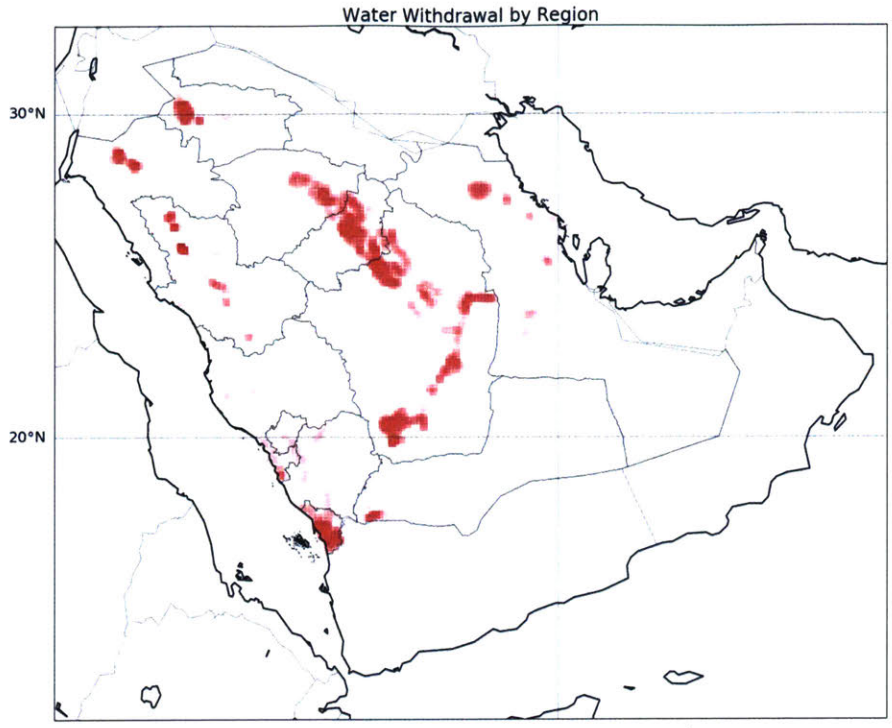

Figure 3-8: Spatial distribution of groundwater withdrawals

discuss groundwater depths in a comprehensive manner, this makes it challenging to estimate the cost of energy required to pump groundwater to the surface. As a proxy to approximate energy requirement, data published by the Saudi Electricity Company (SEC) on electrical power consumed in the agricultural sector is analyzed to come up with the energy intensity of water extraction (mega watt hour/million cubic meter). Not all farmers in Saudi Arabia use grid electricity, and not all grid electricity used in agriculture is for groundwater pumping purposes, but for simplicity, and due to lack of data, the average grid power per cubic meter of groundwater withdrawals is used as a proxy of energy requirements for groundwater extraction. Figure 3-9 shows an increased power intensity of water, that does not necessarily mean increase in water depths, but it is the most likely a contributing reason.

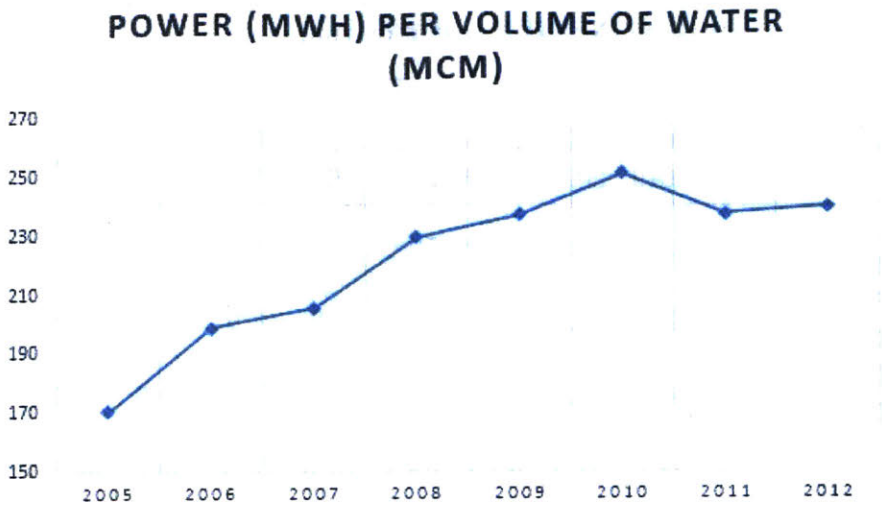

Figure 3-9: Energy Intensity of Agricultural Water Withdrawals

3.4 The Potential of Seawater Desalination for Agriculture

Currently, in 2017, agriculture water demand in Saudi Arabia is fully met through groundwater resources. As the levels of depletion are seemingly not sustainable. The option to use desalinated sea water for agriculture is investigated. Using a graph-theoretic framework called the Interdependent Network Flow with Induced Internal Transformation (INFINIT) model [13, 14]. INFINIT can be used to optimize the flow of water resources and placement of new facilities such as desalination plants and water pipelines (and expansion or retirement of existing facilities) at the individual facility level over multiple dimensions of geographical networks.

To enable running the INFINIT desalination network optimization model, 27 "Agricultural Zones" are created based on clustering areas shown in the map of irrigated areas (Figure 3-7) using a K-mean clustering algorithm. To optimize the water strategy for agricultural demand and municipal demand simultaneously in the INFINIT framework, agricultural zones are added to the baseline network described in [14] as demand nodes. Figure 3-10 places the 27 agricultural zone nodes in the preexisting water desalination infrastructure network as of 2010. It can be seen from

Table 3.1: Desalination for agriculture; Capital costs, operational costs and CO_2 emissions resulting form the INFINIT simulation run.

perios	2010-2014	2015-2019	2020-2024	2025-2029	2030-2034	2035-2039	2040-2044	2045-2049	2050	overall
Total Cost [BUSD/year]	61.6	41.5	65.5	52.3	50.1	52.8	62.9	63.0	75.2	2323.4
CAPEX [BUSD/year]	26.6	2.6	23.0	6.5	1.4	1.2	7.9	4.0	12.8	378.7
OPEX [BUSD/year]	35.0	38.9	42.5	45.8	48.6	51.6	55.0	59.0	62.4	1944.7
Total CO_2 [Mmt/year]	34.3	38.2	42.3	45.6	48.5	51.5	55.1	59.2	64.4	1937.8

the relative size of the demand nodes that the agricultural demand is much larger (an order of magnitude) than the municipal demand.

Figure 3-11 shows the resulting network proposal for 2050 when running an INFINIT multiobjective optimization while setting the objective function to give cost minimization a 50% weight, and 50% weight on minimizing CO_2 emissions. The 2050 water network in Figure 3-11 eventually constitutes a nationwide trans-Arabian-Peninsula pipeline network connecting the east and west coasts. Table 3.1 lists the resulting annual cost and CO2 emission. This model, and its assumptions, are fully documented in a published paper[15].

These results can change greatly depending on the input parameters and assumptions as well as the objective function weights. The cost associated to water desalination for agriculture under the model assumptions is prohibitively high. Agriculture contribution to GDP in 2012 is slightly less than 45 billion Saudi Riyal ($12 Billion) [10]. The model suggests that triple that amount ($35 Billion) is needed as operational costs. There are many ways to reduce those expenses. One approach is to reduce overall agricultural water demand by using higher efficiency irrigation systems, and focusing on crops with less water requirements. Another approach is to reduce water transportation costs by shifting agricultural activity closer to the coastal areas. Doing so is subject to the availability of arable lands within proximity to potential

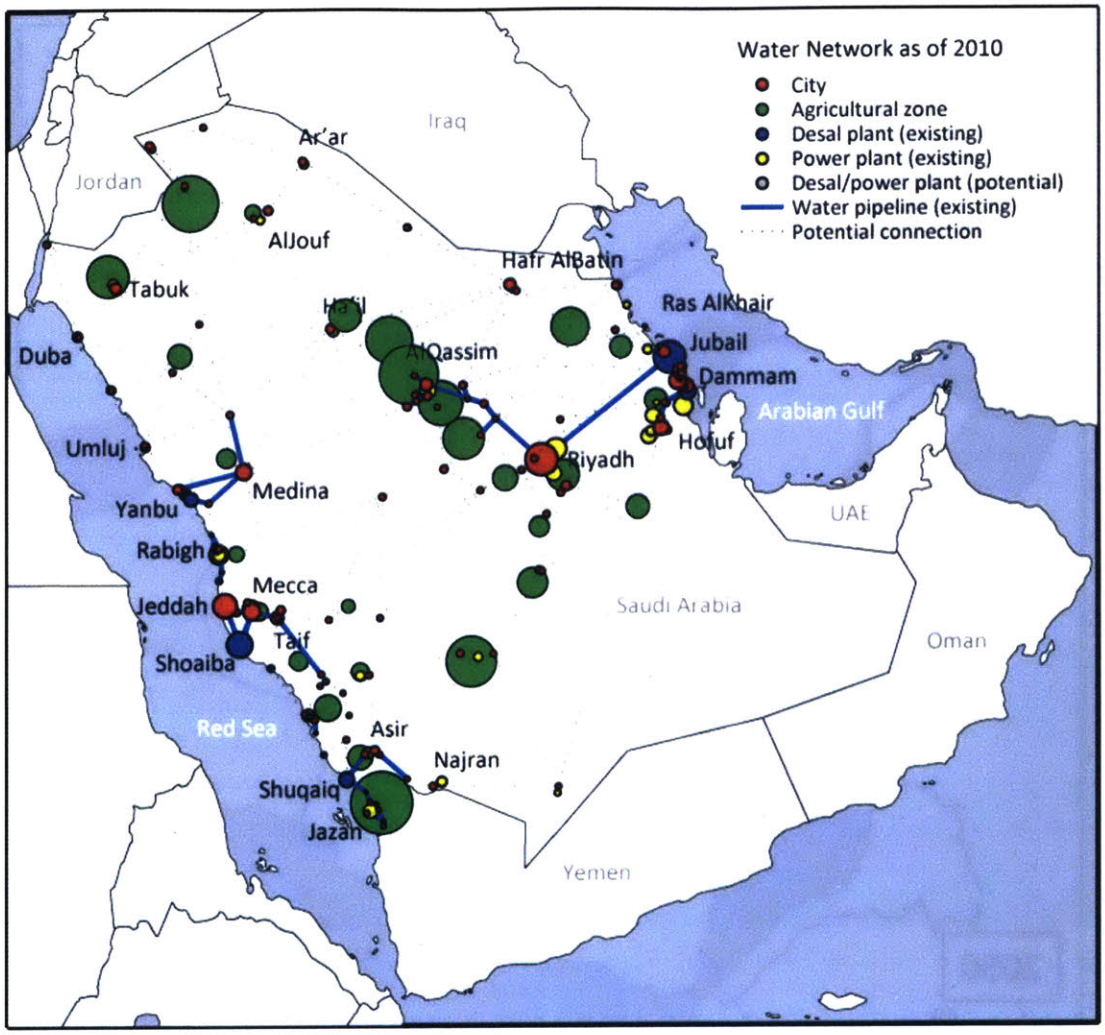

Figure 3-10: 27 agricultural zones, municipal demand nodes and the existing desalination network

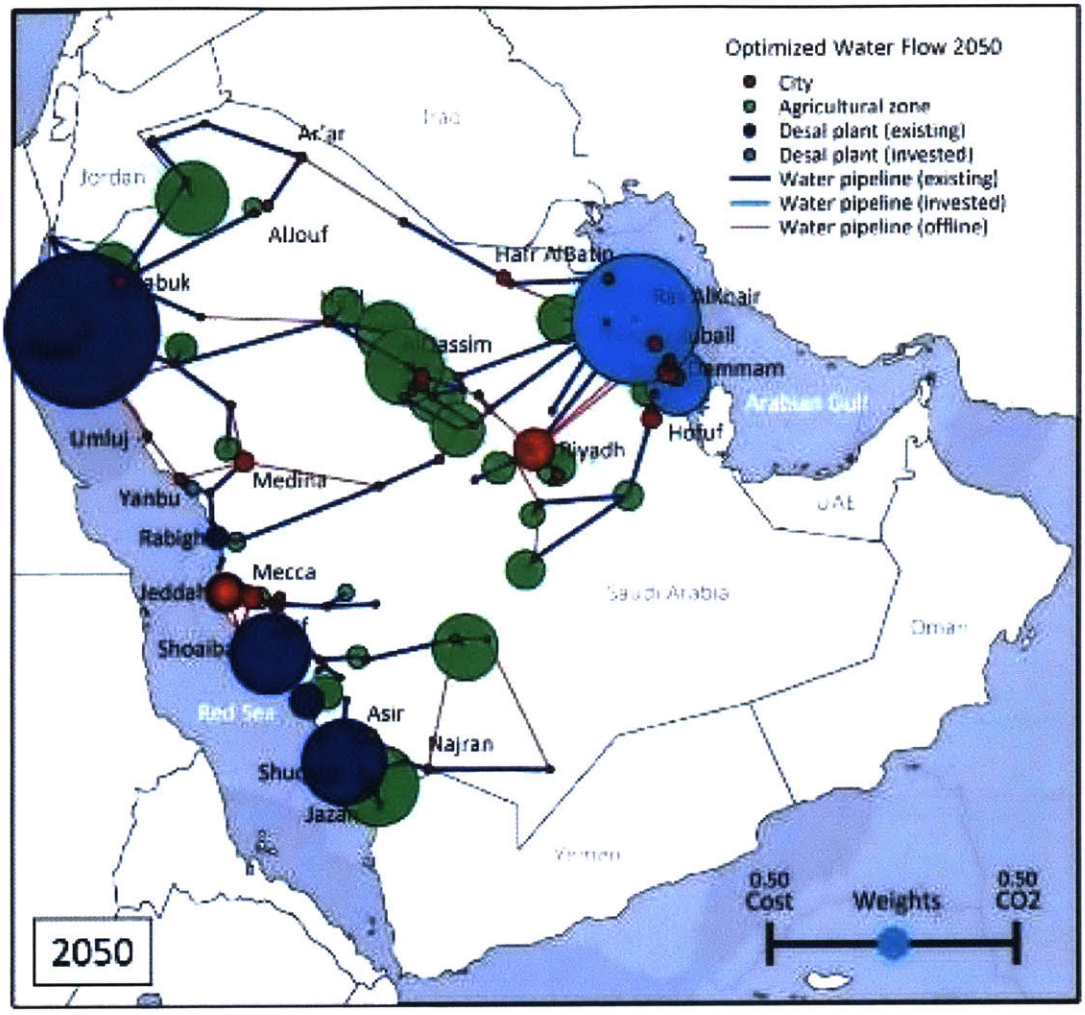

Figure 3-11: The optimized agriculture desalination network at 2050

locations of desalination plants.

3.5 Water Pricing

In this section, three different water valuation metrics are proposed. first, the cost of desalination, and the willingness to desalinate is used. Second, the virtual water concept is used, were food imports act as a proxy to water imports. lastly, farmers willingness to pump groundwater, and the price they pay for electricity are used.

3.5.1 The Cost of Virtual Water Imports

As discussed in Section 3.1.2, Saudi Arabia imported 20 million tonnes in 2015, the cost of those imports was reported to stand at 35 Billion Saudi Riyals [18]. Ignoring any other value contained in those crop imports, and using the assumption that if those crops would have been produced locally under local water requirements, those imports would have needed around 60 BCM. This suggests that the value of a cubic meter of virtually imported water is around 0.6 Saudi Riyal per cubic meter. Figure 3-6 shows a time series of the price of virtual water imports.

3.5.2 The Cost of Groundwater Pumping and the willingness to Pump

In Section 3.3, we showed a lower bound estimation of the electric power needed to pump a cubic meter for agricultural activity. Figure 3-9 shows that the lower bound estimate for the energy requirements for groundwater extraction in 2012 was about 240 Megawatt Hour per Million Cubic Meter (MwH/MCM). Using the subsidized energy price that farmers pay for electricity, which in 2012, was 120 Saudi Arabian Riyals per Megawatt Hour [19], which results in a lower bound cost estimate of 0.028 Saudi Riyals per cubic meter.

3.5.3 The Cost of Desalination and the Willingness to Desalinate

INFINIT, the model that was used to analyze potential of seawater desalination for agriculture in section 3.4, assumes a cost of desalination of 5.6 Saudi Riyals [14]. The cost of seawater desalination depends on many factors, including technology, seawater parameters (Salinity, temperature), climatic parameters (ambient temperature) and policy (Carbon tax, cost to alleviate environmental hazards). In the case of Saudi Arabia, seawater desalination cost also depends on transport cost, as desalination happens in coastal areas and the water needs to be pumped considerable distances and elevation changes to reach inland cities. As an extreme case, using Photo-Voltaic powered Multi-Effect Destination (PV-MED) plant on the red sea, could cost up to 14 Saudi Arabia Riyals as shown in Figure 3-12.

3.5.4 Comparison to Current Tariffs

Municipal water pricing follows a tiered structure, where prior to 2016, that tiered structure ranged between 0.1 and 6.0 Saudi Riyals. A policy rolled out in 2016 changed the tariff range into 0.15 to 9.0 Saudi Riyals [20], and reducing the tier cutoffs considerably. Figure 3-13 compares old tariffs, new tariffs and four of the proposed water pricing.

3.6 Conclusion

In this chapter, the agriculture sector in Saudi Arabia is discussed, where it was shown that agriculture falls behind in many economic parameters such as labor productivity and labor wages compared to other sectors of the economy. Spacial distribution of water requirements in agriculture is studied, allowing for a framework to propose reforms to determine what crops are the most suitable for Saudi Arabia's water balance, and determining the amount of cultivated land area, and investigating the use of more efficient irrigation methods This chapter investigated seawater desalination

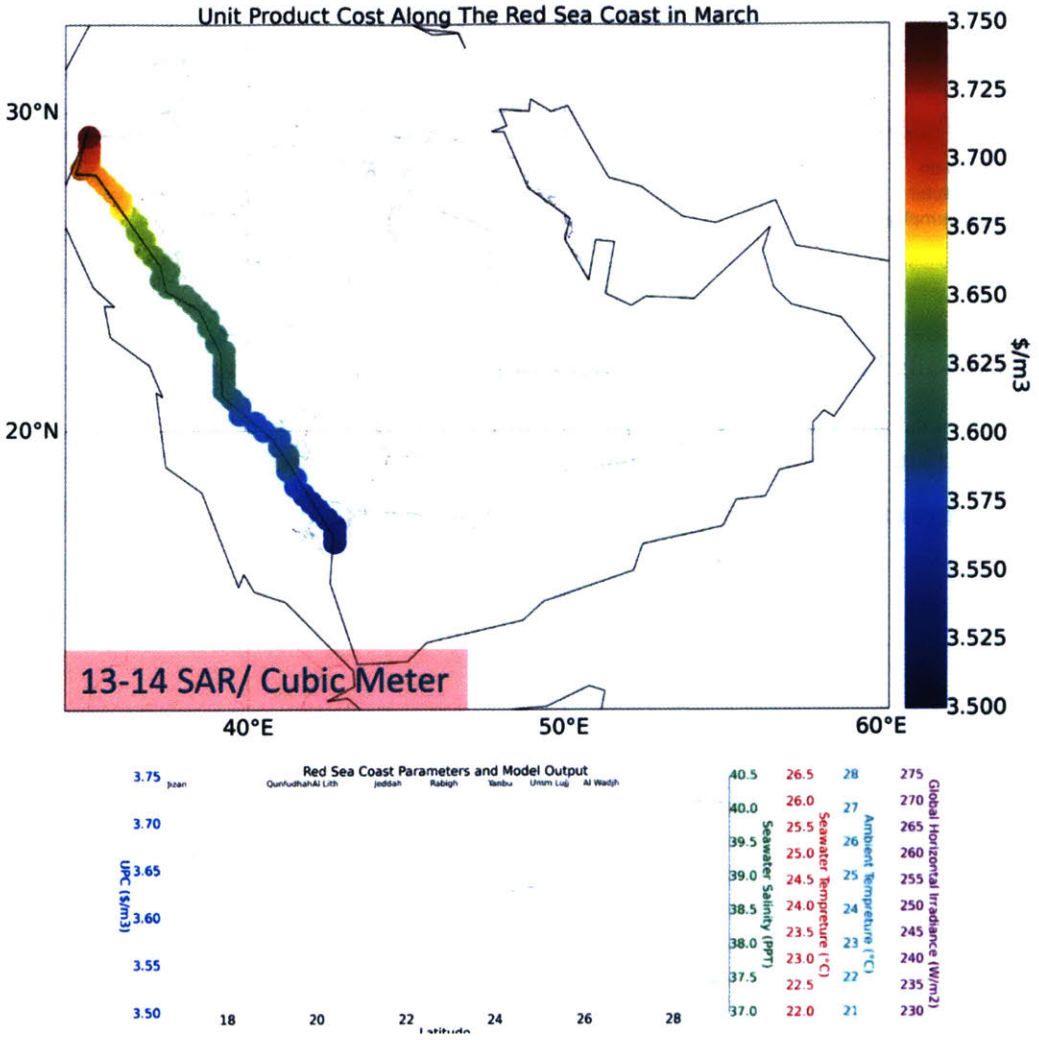

Figure 3-12: The cost of using Photo Voltaic Multi Effect Destination (PV-MED) on the coast of the Red Sea

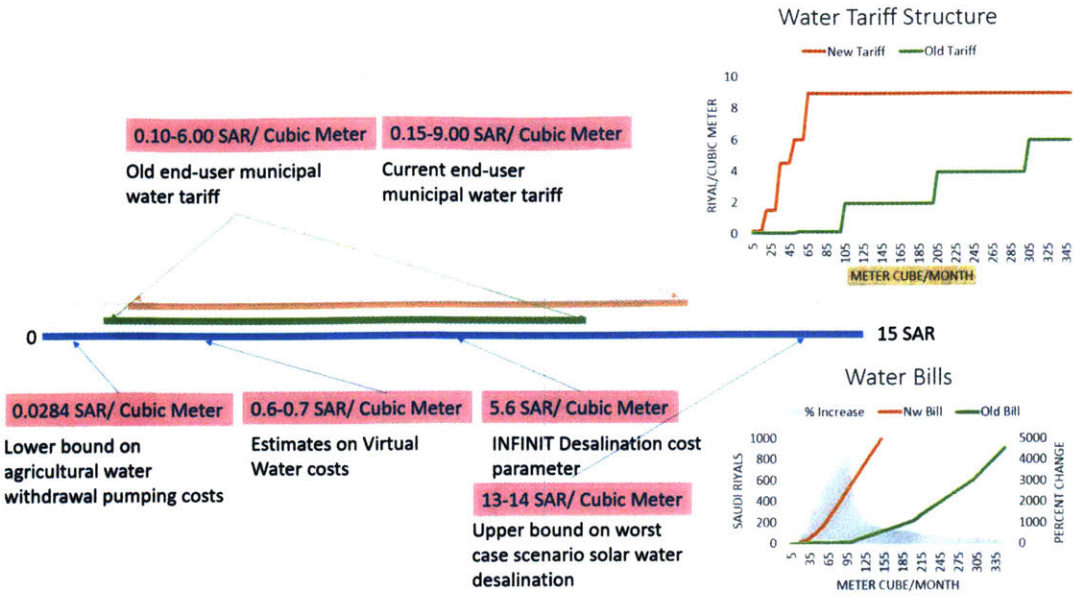

Figure 3-13: Comparing old, new water tariffs to four proposed water pricing metrics

as an option to complement groundwater, and then proposed a set of water pricing mechanisms that were compared with the existing water tariffs in Saudi Arabia.

Chapter 4

Simulating Water Competition Between Municipal and Agricultural Uses in Riyadh

4.1 Background

Riyadh, Saudi Arabia is a city of 5 million people, and it depends for its water supplies on two main sources: groundwater aquifers, and seawater desalination. Desalination is an energy intense process, and the fact that the closest seashore is within 250 miles of the city, seawater desalination and transport is costly. The city tries to utilize whatever groundwater resources it has access to, and the city now gets 40% of its water supplies from eight different well fields that are shown in Figure 4-1. The largest, Alhenny well field, supplies the city a daily average of 400,000 cubic meter, the eight well fields together supply the city an average of a million cubic meter a day (Figure 4-2).

4.2 Simulation Scope

Agricultural activity within proximity to the city taps the same fossil water aquifers that supply the city with water. In this chapter, three agricultural clusters west of

Table 4.1: A list of the eight municipal water wells, and the three agricultural zones, and their corresponding annual water withdrawals

Name	Withdrawal $(m^3)/year$	Lat	Long
Salbukh Water Station	3.18E+07	25.056079	46.479378
Al Hunayy	1.29E+08	24.964418	48.755869
Buwaib Station	3.17E+07	25.027669	46.837671
Al Wasee	7.46E+07	25.097826	47.540069
Manfuhah	2.18E+07	24.600296	46.717285
Al Malaz	4.97E+06	24.676511	46.723169
Ash Shimaisi	1.02E+07	24.623568	46.703326
Al Hair	1.78E+07	24.355362	46.907451
Agricultur Zone 1	1.05E+08	24.04666667	45.44666667
Agricultur Zone 2	2.20E+08	24.64230769	45.83076923
Agricultur Zone 3	2.44E+08	24.271875	46.0875

the city are looked at, and the impact of agricultural water withdrawals on limiting the resources available to the city is analyzed.

The scope of this analysis is the groundwater system of the city of Riyadh, which includes many elements. Throughout this analysis, all those elements are assumed to tap one single continuous aquifer with uniform and isotropic characteristics such as conductivity and storativity. This aquifer is accessed by these elements:

- 8 municipal water supply well fields
- 3 agricultural clusters

Those elements are shown spatially in Figure 4-1. Annual withdrawal amounts that are used as inputs to the model presented in this paper are shown in Table 4.1. The single aquifer assumption is a major simplification, and does not reflect actual conditions in the area. Different well fields and agricultural zones might tap into multiple, sometimes overlaying aquifers.

In this analysis, the goal is to explore the interaction between the list of withdrawal points listed in Table 4.1, specifically, it is important to understand the significance of the effect of agricultural activity on the city's water resources. the study compares the current state, where agricultural activity consumes a significant amount of the city's groundwater resources, to a scenario where there is no agricultural activity. How

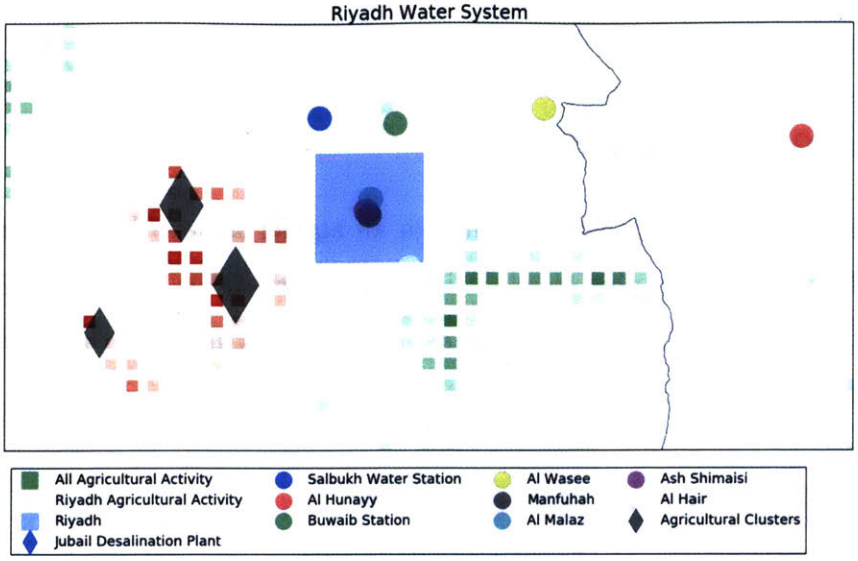

Figure 4-1: The location of eight well fields supplying Riyadh, Saudi Arabia is shown by the eight circles, the city is shown by the blue square, and the analyzed three agricultural clusters are shown as black diamonds.

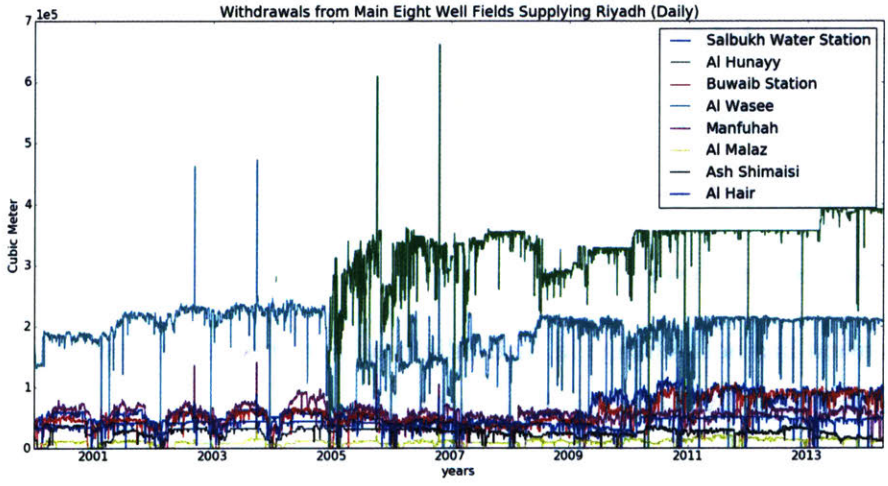

Figure 4-2: Historical daily water withdrawals from the eight well fields

would that influence the extraction capacity of municipal water supply well fields, and the overall state of the aquifer? The level of hydraulic head, h, is focus of this chapter.

4.3 Governing Equations

In hydrology, flow of groundwater through an aquifer is described by the **groundwater flow equation**; this equation is usually derived for a small Representative Element Volume (REV) in which we assume constant medium properties such as aquifer transmissivity and storativity.

4.3.1 Groundwater flow equation

We can describe the transient flow of groundwater as a diffusion equation, similar to the well studied heat transfer equation, The groundwater flow equation then becomes:

$$S_s \frac{\partial h}{\partial t} = -\nabla \dot{q} - G$$

where :

- h: Hydraulic head in an aquifer, it can physically be measured as the depth of the well needed to access groundwater.
- S_s: specific storage
- q: divergence of the flux
- G: source/sink term

This equation has both change in hydraulic head and flux as unknowns, Darcy's law that relates flux to hydraulic head is substituted:

$$q = -\kappa \nabla h$$

Where:

- κ: hydraulic conductivity

Assuming that a uniform and isotropic κ: hydraulic conductivity, the groundwater flow equation becomes:

$$S_s \frac{\partial h}{\partial t} = \kappa \nabla^2 h - g$$

We divide both sides by S_s: specific storage, to obtain:

$$\frac{\partial h}{\partial t} = \alpha \nabla^2 h - G$$

Where:

- $\alpha = \kappa / S_s$: hydraulic diffusivity

in three dimensional Cartesian coordinates, we have:

$$\frac{\partial h}{\partial t} = \alpha [\frac{\partial^2 h}{\partial x^2} + \frac{\partial^2 h}{\partial y^2} + \frac{\partial^2 h}{\partial z^2}] - G$$

4.4 Methodology

To solve this problem, we opt to use a finite difference scheme, we apply Taylor series expansion for the function h along the x, y and z axes, we show the expansion along the x axis:

$$
\begin{aligned}
h(x+\Delta x, y, z) =& h(x, y, z) \\
&+ \frac{\Delta x}{1} \frac{\partial h(x, y, z)}{\partial x} \\
&+ \frac{\Delta x^2}{2} \frac{\partial^2 h(x, y, z)}{\partial x^2} \\
&+ \frac{\Delta x^3}{6} \frac{\partial^3 h(x, y, z)}{\partial x^3} + \ldots \\
h(x-\Delta x, y, z) =& h(x, y, z) \\
&- \frac{\Delta x}{1} \frac{\partial h(x, y, z)}{\partial x} \\
&+ \frac{\Delta x^2}{2} \frac{\partial^2 h(x, y, z)}{\partial x^2} \\
&- \frac{\Delta x^3}{6} \frac{\partial^3 h(x, y, z)}{\partial x^3} + \ldots
\end{aligned}
$$

We sum up the two Taylor series expressions to get:

$$
\begin{aligned}
h(x-\Delta x, y, z) + h(x+\Delta x, y, z) =& 2h(x, y, z) \\
&+ \frac{\Delta x^2}{1} \frac{\partial^2 h(x, y, z)}{\partial x^2} \\
&+ \frac{\Delta x^4}{12} \frac{\partial^4 h(x, y, z)}{\partial x^4} \\
&+ \ldots
\end{aligned}
$$

Giving:

$$
\begin{aligned}
\frac{\partial^2 h(x, y, z)}{\partial x^2} =& \frac{h(x-\Delta x, y, z) + h(x+\Delta x, y, z) - 2h(x, y, z)}{\Delta x^2} \\
&- \frac{\Delta x^2}{12} \frac{\partial^4 h(x, y, z)}{\partial x^4} + \ldots \\
&= \frac{h(x-\Delta x, y, z) + h(x+\Delta x, y, z) - 2h(x, y, z)}{\Delta x^2} \\
&+ O(\Delta x^2)
\end{aligned}
$$

And therefore, in second order accuracy:

$$\frac{\partial^2 h}{\partial x^2} \approx \frac{h(x-\Delta x, y, z) + h(x+\Delta x, y, z) - 2h(x, y, z)}{\Delta x^2}$$

Similarly, for the y and z dimensions:

$$\frac{\partial^2 h}{\partial y^2} \approx \frac{h(x, y-\Delta y, z) + h(x, y+\Delta y, z) - 2h(x, y, z)}{\Delta y^2}$$
$$\frac{\partial^2 h}{\partial z^2} \approx \frac{h(x, y, z-\Delta z) + h(x, y, z+\Delta z) - 2h(x, y, z)}{\Delta z^2}$$

Setting a uniform discrimination over the domain $[0, ..., R]$ and a number of points m along each dimension:

$$\Delta x = \Delta y = \Delta z = \frac{R}{m}$$

We establish the following boundary conditions:

$$\frac{\partial h(0, y, z)}{\partial x} = \frac{\partial h(R, y, z)}{\partial x} = \frac{\partial h(x, 0, z)}{\partial y} = \frac{\partial h(x, R, z)}{\partial y} = 0$$

Implementing this scheme into matrix form, yields the A matrix shown in Figure 4-3; and this system is needed to be solved:

$$A \begin{bmatrix} h_{1,1,1} \\ \dots \\ h_{m,1,1} \\ h_{1,2,1} \\ \dots \\ h_{m,m,1} \\ h_{m,m,2} \\ \dots \\ h_{m,m,m} \end{bmatrix} = \begin{bmatrix} G_{1,1,1} \\ \dots \\ G_{m,1,1} \\ G_{1,2,1} \\ \dots \\ G_{m,m,1} \\ G_{m,m,2} \\ \dots \\ G_{m,m,m} \end{bmatrix}$$

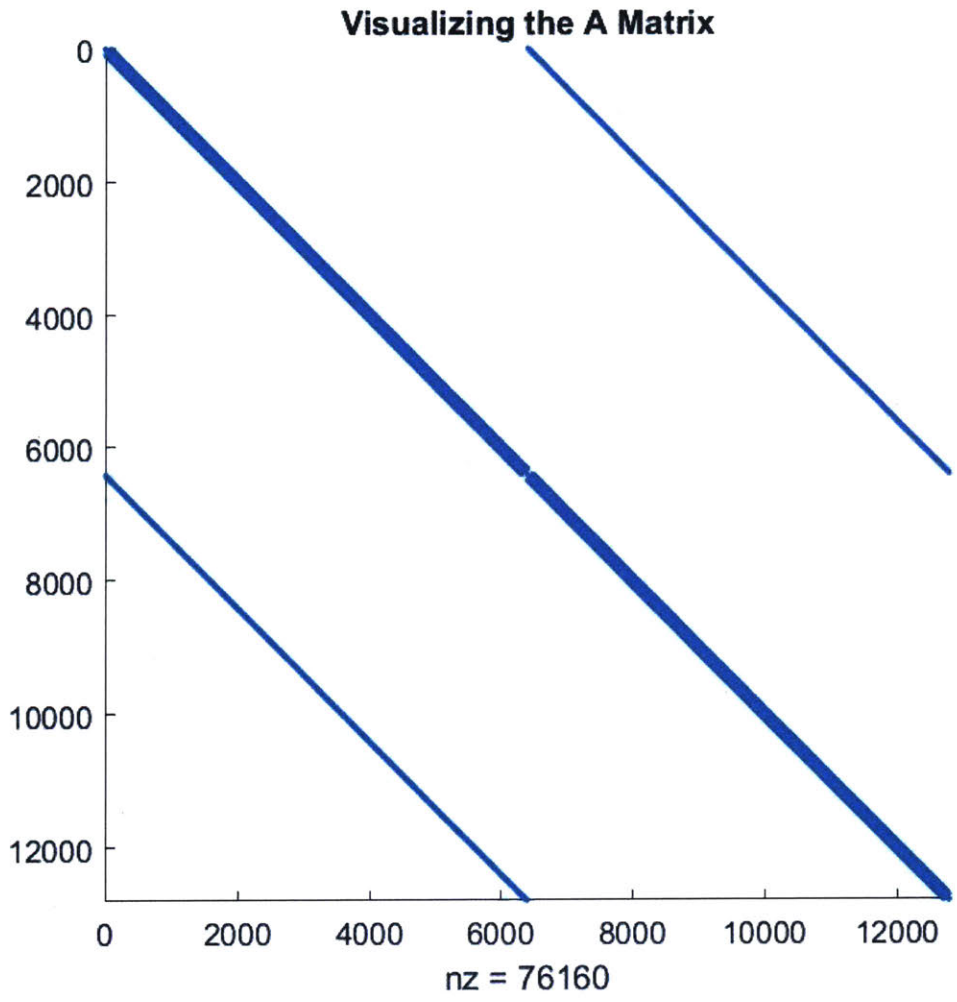

Figure 4-3: Visualizing the A matrix resulting form a central difference discretization

4.5 Accuracy Estimation

The finite difference scheme discussed earlier is analyzed in order to estimate the accuracy by performing a grid refinement study, as it is not possible to obtain an analytic solution. The grid refinement study give confidence that the obtained solution is grid-converged. an extremely fine grid is simulated and then compared to a set of a coarser grid solutions. This shows that the used finite difference scheme is second order accurate, a convergence plot displaying the error verses the number of elements shows a line on a log-log plot with a slope of minus two. it means that an increase of the number of elements by one order of magnitude, reduces the error two orders of magnitude. This plot is shown in Figure 4-4

4.6 Results

We use the scheme developed here to run two simulations:

- **Simulation 1 - City With Agriculture**: In this simulation, the aquifer is assumed to be drawn from by all the 8 municipal supply wells and the 3 agricultural clusters shown in Table 4.1 and Figure 4-1. This shows the current situation of the city as it is. We use one year worth of water withdrawals as an input to the model.

- **Simulation 2 - City Without Agriculture**: In this simulation, all agricultural activity is stopped, and only let the aquifer be drawn from by municipal supply water wells: the first eight entries in Table 4.1, the circles in Figure 4-1. There is no agricultural activity in this scenario.

The results of **Simulation 1** are shown in Figure 4-5; It is observable in the figure, that a significant drop in hydraulic head in the southwest part of the analyzed region where the three agricultural clusters are concentrated. The model estimates the drop in hydraulic head in the southwest region to reach 36 meters a year. In the same simulation, we see a drop of the water table in the northeast part of the

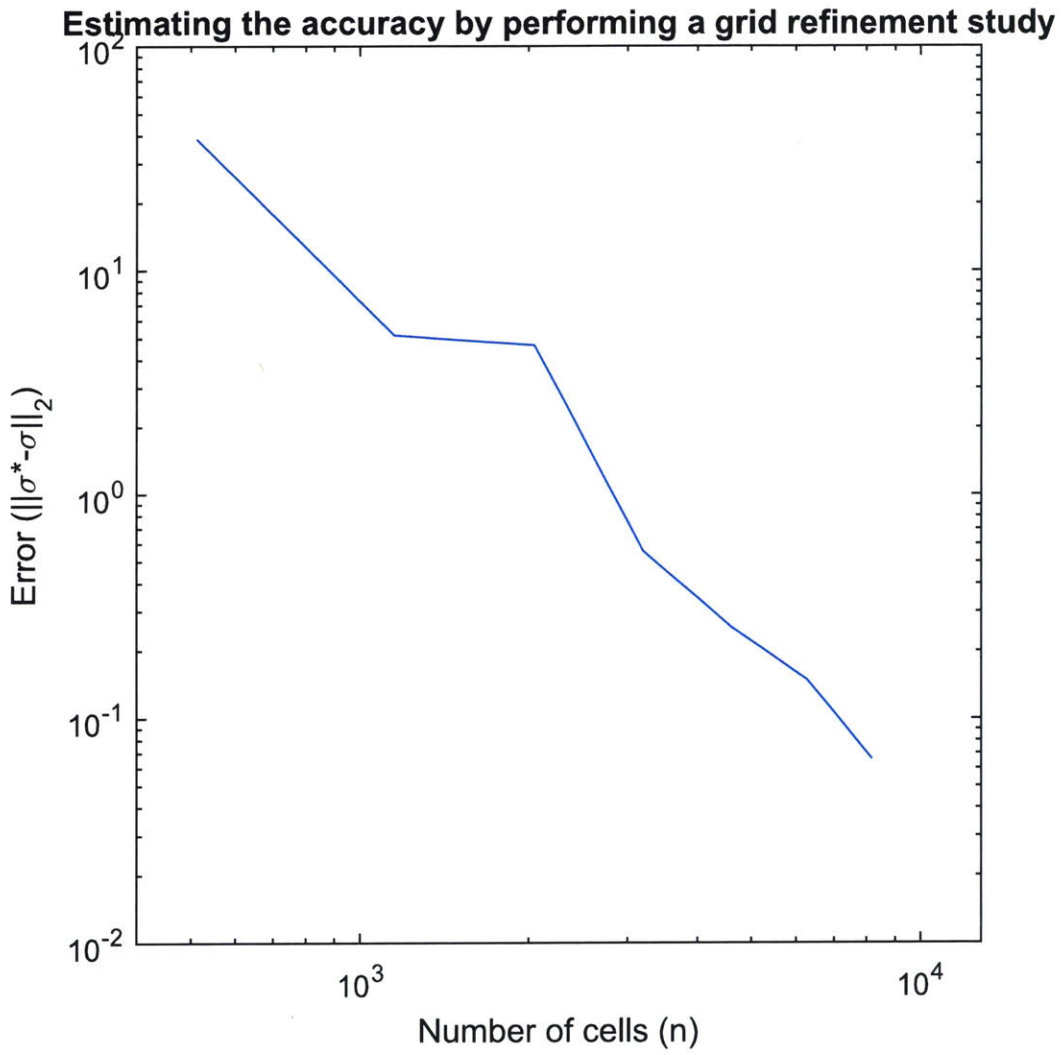

Figure 4-4: The result of running a grid refinement study to the finite differences scheme

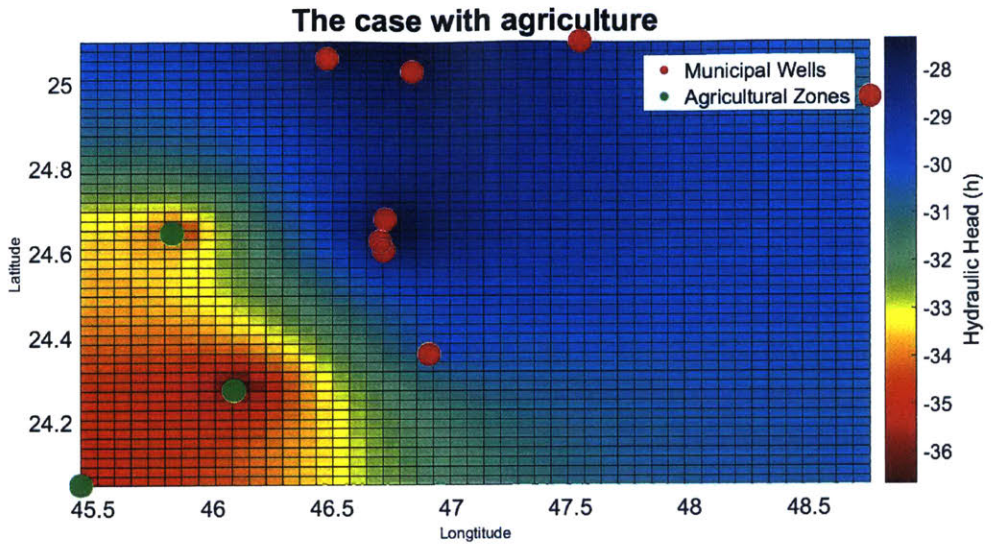

Figure 4-5: Results of the simulation showing the water level for the current situation, full agricultural activity and municipal water demand.

area by 31 meter. That part is where the "Al Hunayy" municipal water well field is located. This is the largest supplier of fresh water to the city. The rest of the area witnessed an average drop of 27 meters, as a result from the withdrawals from both the agriculture and municipal water wells.

The results of **simulation 2** are shown in Figure 4-6. This simulation assumes no agricultural activity, and the significant impact of the "Al Hunayy" municipal water well field is clearly identifiable, as it is visible in the northeast corner of the area. The drop there is about 15 meters per year, as opposed to 31 meters per year in the case of agricultural activity. Other areas in the map averaged a drop of 10 meters per year.

To analyze the significance of agricultural activity, the difference between the two simulation is taken, this is shown in Figure 4-7. This figure shows the drop of the hydraulic head that is directly caused by agriculture. The model estimates the impact of agriculture to be an annual drop of around 26 meters per year in the southwest area, where agricultural activity happen. This gradually decrease until it reaches 16 meters per year in areas away from the agricultural zone.

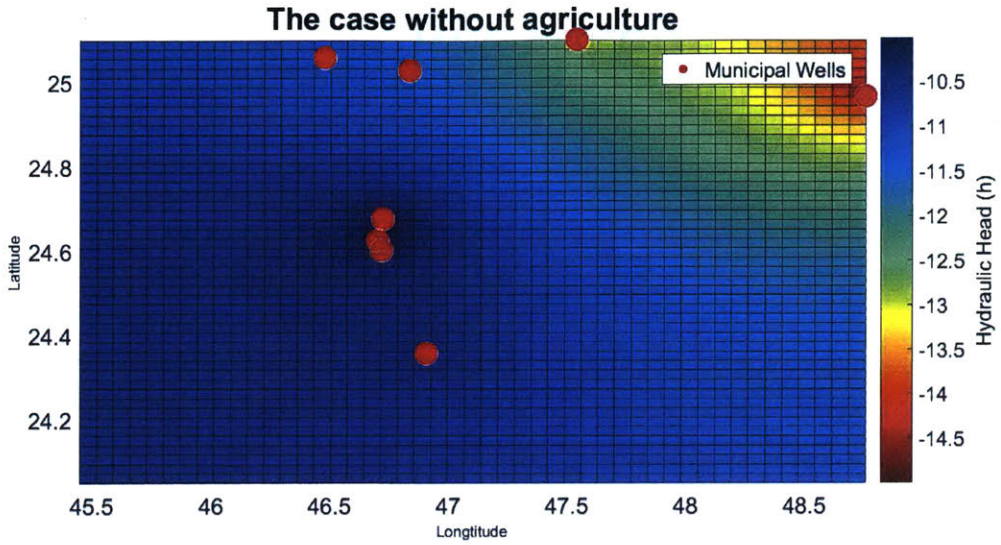

Figure 4-6: Results of the simulation showing the water level for the proposed scenario of limiting agricultural activity and only keeping municipal water demand.

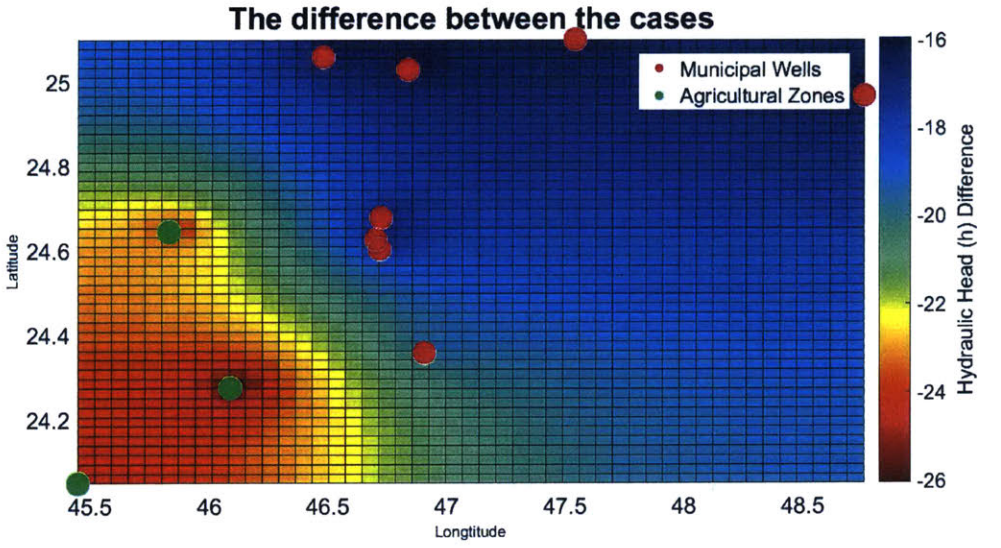

Figure 4-7: The difference between the two simulations, this figure shows the drop in hydraulic head due to agricultural activity.

4.7 Conclusions

in this chapter, a finite difference approach is used to discretize the groundwater flow equation. The intention was to study the dynamics of the eight groundwater well fields that supply the city of Riyadh, and the three agricultural zones that are within proximity to the city. Due to data limitations on the specific boundary of the aquifers, and the initial water head, some simplifying assumptions were made:

- We assumed that the city and the surroundings gets it water from one single aquifer. In reality, the entries in Table 4.1 are connected to different aquifers at different depths, and different geographical layers.

- The model only considers a small bounded area of around 60Km by 60Km. The actual aquifers are much larger, and extend for hundreds of kilometers, thus, enclose significantly larger volumes of water. This led to an exaggerated drops of hydraulic head in this model.

- It is not just the city that depends on this aquifer system, as the aquifers are extensive in geographical coverage, the national municipal and agricultural activity is all competing to get access. A comprehensive model that include more elements such as the one showed in Figure 4-8 should be used in order to gain actionable insights.

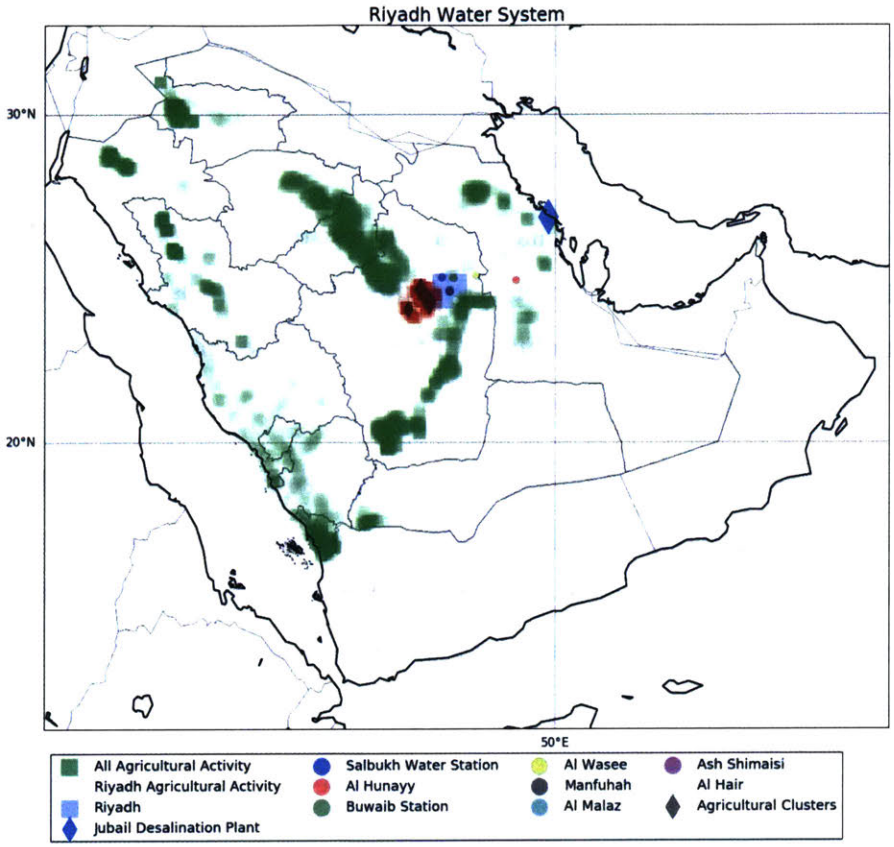

Figure 4-8: The national agricultural system, the elements studied in this analysis appear in the central region, and they only constitute a small fraction of the national system..

Chapter 5

Cost-Optimizing Photovoltaic Powered Electrodialysis Reversal (PV-EDR) Systems for Off-Grid Settings [1]

5.1 Introduction

Throughout the world, brackish groundwater is more prevalent than fresh groundwater. The ability to produce potable, desalinated groundwater in off-grid settings is particularly critical in developing countries, where more than 600 million people lack access to a safe water source. PV-EDR has the potential to provide a disruptive, economically sustainable water solution in off-grid communities. PV-EDR reduces the energy consumption of brackish groundwater per unit volume of product water by half compared to reverse osmosis (RO), and improves recovery of input water from 40% to up to 95%. A significant gap in PV-EDR technology is the availability of PV subsystems that are both low-cost and optimized to power an EDR system. This

[1] This chapter has been written in collaboration with David W. Bian and Sterling M. Watson from the Department of Mechanical Engineering at MIT as the final project in the 16.888 course taught in Spring 2016. Multidisciplinary System Design Optimization course staff: Professor Olivier de Weck and TA Sydney Do.

gap is critical, as low-cost solutions are necessary to provide scalable, sustainable desalination to remote communities. In this chapter, we present the results of several multidisciplinary system design optimization methods applied to the PV-EDR desalination system, to arrive at a cost-minimal integrated design of the PV power and EDR desalination subsystems.

5.1.1 Background

Optimization methods have been applied to the design of PV-powered desalination systems in recent work. Bourouni *et al* [24] used a genetic algorithm (GA) to generate several possible designs for coupling a small brackish water RO system to a combination of renewable energy sources, namely solar PV and wind turbines. The objective of this optimization was to minimize the total cost, including capital and operational costs, using various combinations of components. Designs with and without batteries, and with PV, wind turbine, and hybrid power system configurations were obtained using the optimization and applied to a specific test site in Ksar Ghilène, Tunisia. Koutroulis *et al* [26] proposed a methodology for sizing a hybrid PV and wind turbine-powered RO system to minimize 20-year total system cost. A genetic algorithm was used for the cost function minimization, and was used to design a community-scale and residential-scale desalination system. The optimization considered various combinations of RO desalination units, PV panels, wind turbine generators, and batteries as design variables. In Kim *et al* [25], a genetic algorithm was used to optimize a community-scale PV-RO desalination system for case studies in the Red Sea and Sinai regions, looking at seawater and brackish water applications. The number of RO components, ratio of battery storage to nameplate PV power output, and power control variables were used in conjunction with first-order cost models and location-specific environmental data to create the PV-RO cost model. The work presented here differs from what has been found in the literature in that it considers operating time as a design variable, uses gradient-based and particle swarm optimization methods, and uses electrodialyis reversal as the technology of choice for community scale, brackish water desalination.

5.1.2 EDR vs. RO

Reverse osmosis is one of the most commonly used desalination technologies. It is a membrane desalination process that separates high salinity and low salinity solutions through the use of semi-permeable membranes, by applying pressure to the solution against the osmotic pressure as shown in Figure 5-1.

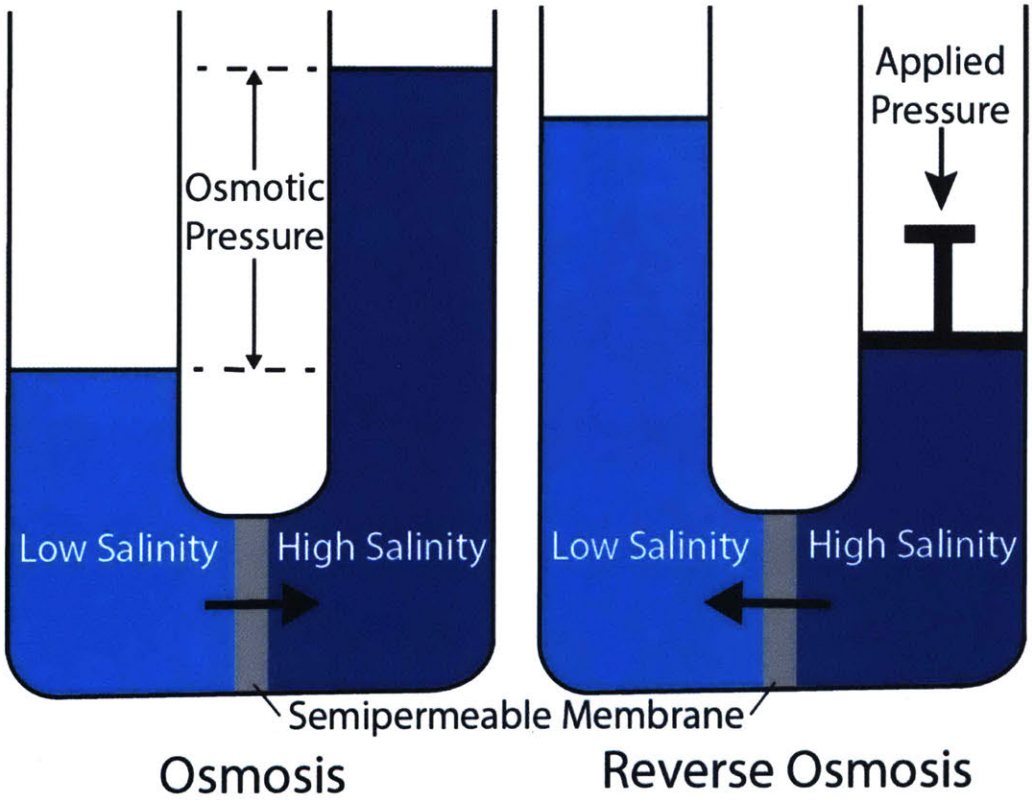

Figure 5-1: Reverse osmosis. [28]

Electrodialysis (ED) has emerged as a promising membrane desalination technique. In the ED process, feed water is pumped along a series of alternating anion and cation exchange membranes (AEM and CEM). The layered configuration of these membranes is called a "stack". An electric potential is applied across the stack, forcing the anions toward the anode and cations toward the cathode. Because the AEM allows anions to pass while blocking cations, and the CEM allows cations to pass while blocking anions, alternating streams of diluted and concentrated saline water

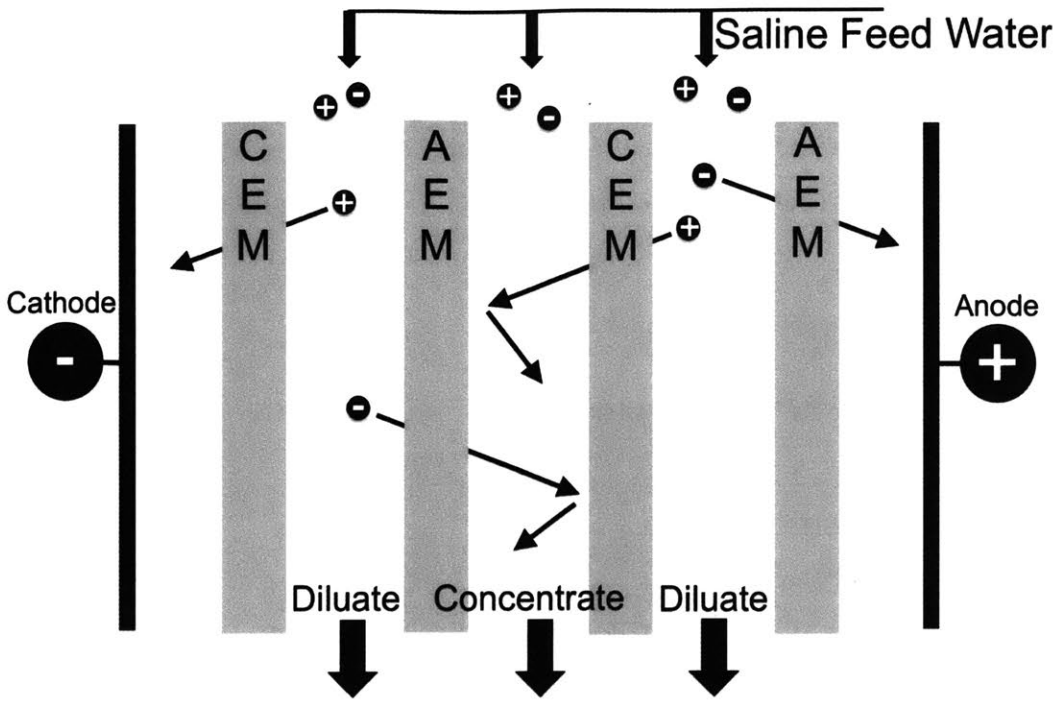

Figure 5-2: Electrodialysis.[28]

are created within the stack. This process is depicted in Figure 5-2. Electrodialysis reversal (EDR) is the same process as ED with the exception that the electric potential is reversed at a given time interval to minimize fouling of the membranes, thereby increasing their lifetimes.

For the salinity levels of the brackish groundwater available in Saudi Arabia, ED has several compelling advantages compared to RO. The energy consumption of ED per unit volume of product water is roughly 25% to 75% of the energy required when using RO. This means that a PV-EDR system requires a smaller and thus less expensive power system than that of an analogous PV-RO system. Recovery rate, the volumetric ratio of product water to feed water, is particularly important in water-stressed areas like Saudi Arabia. The recovery rate of ED is about 95%, compared to 30-50% for RO, meaning that ED wastes less water than RO. Lastly, ED membranes have lifetimes of 10-15 years, whereas RO membranes have lifetimes of 3-5 years. An ED-based system requires less frequent membrane replacements, thereby reducing the recurring costs of the desalination system.

5.1.3 PV Power Source

The primary power sources for small-scale, off-grid desalination are solar PV, wind generators, and diesel generators. Due to its long operating lifetime and minimal maintenance and recurring costs, solar PV is particularly appealing for remote off-grid desalination applications. Furthermore, desalination is an energy-intensive process, so powering it with an this abundant and renewable energy source makes a case for desalination as a sustainable source of freshwater. For these reasons, solar PV is chosen as the power source for the EDR desalination system in this optimization.

5.2 System Model

5.2.1 Overview

The PV-EDR system is composed of two subsystems: the PV power subsystem and EDR desalination subsystem, which are modeled separately and are related by the common language of power and daily operating time. The components considered in this analysis are the area of PV panels, amount of batteries required for energy storage, and number of EDR cell pairs for desalination.

EDR Subsystem Model

The electrodialysis subsystem model is characterized by the relationship between the applied voltage and current through the stack as well as the mass balance for diluate and concentrate tanks and cells. These relationships can be described by the following equations:

$$V_{total} = V_{electrode} + NV_{potential} + Ni(R_{dil} + R_{conc} + R_{AEM} + R_{CEM}) \tag{5.1}$$

where V_{total} is the total applied voltage, $V_{electrode}$ is the electrode potential, $V_{potential}$ is the concentration potential, N is the number of cell pairs (each composed of an

AEM and CEM) in the stack, i is the area current density and R_{dil}, R_{conc}, R_{AEM} and R_{CEM} are the area electrical resistances of the diluate stream, concentrate stream, AEM and CEM, respectively.

Assuming that the thickness of Nerst diffusion layer, δ, is negligible compared to the membrane gap, L, and that concentration is homogeneous inside the compartment and water conductivity is negligible, the diluate compartment resistance can be calculated by the following equation:

$$R_{dil} = \rho \frac{L - 2\delta}{A} \cong \frac{1}{C_{dil}\Lambda_{dil}} \frac{L}{A} \tag{5.2}$$

and the analogous equation can be used to find the concentrate compartment resistance. Λ_{dil} is the molar conductivity and can be found using the Falkenhagen equation:

$$\Lambda_{dil} = \Lambda_0 - (B_1\Lambda_0 + B_2)\frac{C_{dil}^{0.5}}{1 + B_0 u C_{dil}^{0.5}} \tag{5.3}$$

where Λ_0 is the molar conductivity at infinite dilution (Sm^2/mol), u is a temperature-independent parameter (Å), and B_0, B_1, B_2 are dimensionless numbers, known for aqueous solutions at a wide range of temperatures.

The following equations depict the mass balance within the tanks:

$$\frac{dC_{dil}^{in}}{dt} = \frac{Q_{dil}}{\forall_{dil}^{tank}}(C_{dil}^{out} - C_{dil}^{in}) \tag{5.4}$$

$$\frac{dC_{conc}^{in}}{dt} = \frac{Q_{conc}}{\forall_{conc}^{tank}}(C_{conc}^{out} - C_{conc}^{in}) \tag{5.5}$$

where C^{in} and C^{out} are the concentrations of the streams as they enter and exit the stack, respectively, $\forall^{tank}$ is the volume of a tank and Q is the volumetric flow rate of the streams.

For the two following equations, the derivation from fundamental equations can be found in [29], and the final form as given can found in [30].

$$\frac{dC_{dil}^{out}}{dt} = \frac{1}{N\forall_{cell}}[Q_{dil}(C_{dil}^{in} - C_{dil}^{out}) - \frac{N\phi I}{zF} + \frac{NAD_a(C_{conc}^{AEM} - C_{dil}^{AEM})}{l_a} + \frac{NAD_c(C_{conc}^{CEM} - C_{dil}^{CEM})}{l_c}]$$

$$\frac{dC_{conc}^{out}}{dt} = \frac{1}{N\forall_{cell}}[Q_{conc}(C_{conc}^{in} - C_{conc}^{out}) + \frac{N\phi I}{zF} - \frac{NAD_a(C_{conc}^{AEM} - C_{dil}^{AEM})}{l_a} - \frac{NAD_c(C_{conc}^{CEM} - C_{dil}^{CEM})}{l_c}]$$

where $\forall_{cell}$ is the volume of a cell, ϕ is the current efficiency, I is the current, z is the ion charge, F is Faraday's constant, l_a and l_c are the thicknesses of the AEM and CEM, D_a and D_c are the diffusion coefficients of the given solution in the AEM and CEM, and C_{dil}^{AEM}, C_{dil}^{CEM}, C_{conc}^{AEM} and C_{conc}^{CEM}, C_{dil}^{AEM} and C_{dil}^{CEM} are the concentrations of the diluate and concentrate streams where they interface with the AEM and CEM. The first term represents the ions entering and exiting, the second term represents the migration of ions between the diluate and concentrate streams due to the electric potential, and the last terms represent the back diffusion due to the concentration gradient across the membranes.

Given a specific operating time t_{op} (h) and daily water requirement V_{wdaily} (m^3), Q_{dil} is given by:

$$Q_{dil} = \frac{V_{wdaily}}{t_{op}} \tag{5.6}$$

Combined with the feed water and target salinity level, these equations form the basis for calculating the number of cell pairs N and the EDR subsystem power requirement, which is then fulfilled by the PV power subsystem.

PV Power Subsystem Model

The power system consists of PV solar panels and energy storage in the form of batteries. Figure 5-3 graphically shows how the required battery capacity is found based on the operating time, area of PV panels, solar irradiance, and PV efficiency.

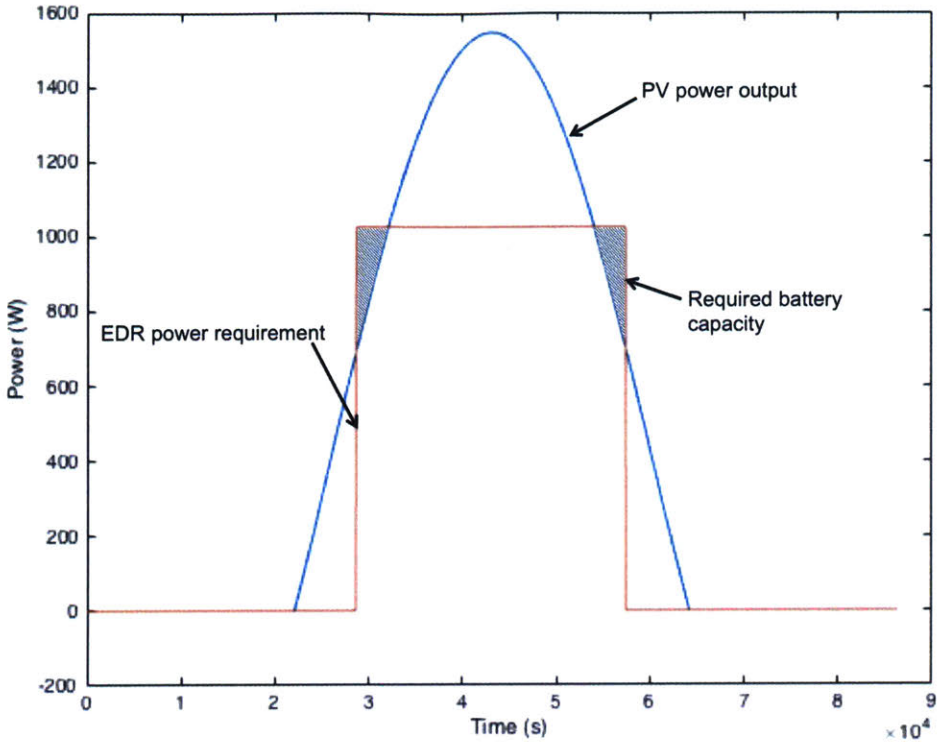

Figure 5-3: Graphical depiction of the PV power system model. The parabolic curve is the PV power output over the course of a day. The rectangular curve is the EDR power requirement. The shaded area represents the required energy storage capacity for this design configuration.

The parabolic curve is the PV power output over the course of a day, and is determined by the solar irradiance, PV efficiency, and area of PV panels. Changing any of these variables will scale the curve vertically. The rectangular curve is the EDR power requirement, which is determined by the operating time and corresponding power requirement. Since the amount of water to be desalinated is held constant, the EDR energy is constant. If the operating time were increased, for example, the required power level would decrease accordingly to maintain constant energy. The shaded area is the area in which the EDR power requirement is higher than the power provided by the PV panels, and is the required energy storage capacity for this design configuration.

5.2.2 Optimization Problem Formulation

Design Variables

Two continuous design variables were considered, t_{op} and $A_{PV,extra}$. t_{op} is simply the number of hours per day that the EDR subsystem will run. The total solar panel area in m^2 in the design configuration is represented by

$$A_{PV} = A_{PV,min} + A_{PV,extra} \tag{5.7}$$

where $A_{PV,min}$ is minimum area of solar panels required to produce the total energy required by the EDR subsystem and $A_{PV,extra}$ is the area of solar panel area in excess of $A_{PV,min}$.

Parameters

The parameters associated with the PV subsystem, EDR subsystem, and cost are summarized in Tables 5.1, 5.2, and 5.3 respectively.

Objective Functions

The two objective functions considered in this analysis are initial capital cost J_1 and additional recurring cost J_2 assuming a 20-year lifetime.

$$J_1 = N_{EDR}Cost_{EDR} + E_{battcap}Cost_{batt} + A_{PV}Cost_{PV} \tag{5.8}$$

$$J_2 = N_{EDR}Cost_{EDR}RF_{EDR} + E_{battcap}Cost_{batt}RF_{batt} + A_{PV}Cost_{PV}RF_{PV} \tag{5.9}$$

where N_{EDR} is the number of cell pairs in the EDR stack, $E_{battcap}$ is the required battery capacity, A_{PV} is the required area of solar panels and RF is the replacement frequency over a 20-year lifetime.

Parameter	Description	Value
$irrad(t)$	Time-resolved solar irradiance over 1 day	Varies, W/m^2
η	PV efficiency	15%

Table 5.1: PV Subsystem Parameters

Parameter	Description	Value
V_{wdaily}	Daily water requirement	10 m^2
C_{feed}	Feed water salinity	2000 ppm
C_{prod}	Product water salinity	200 ppm
RR	Recover ratio	85 %
m_{molar}	Molar mass	58.4428 g/mol
A_{spacer}	Spacer cross-section	0.00014974 m^2
v_{linear}	Linear flow velocity	0.06319637 m/s
L	Membrane gap	0.00079 m
$V_{electrode}$	Electrode voltage	2 V
A	Active membrane area	0.34 m^2
L_a	AEM thickness	0.0005 m
L_c	CEM thickness	0.0006 m
R_a	AEM resistance	7 Ωcm^2
R_c	CEM resistance	10 Ωcm^2
D_a	AEM diffusion coefficient	$3.28x10^{-9}$ m^2/s
D_c	CEM diffusion coefficient	$3.28x10^{-9}$ m^2/s
ϕ	Current efficiency	0.88
z	Ion current	1
Λ_0	Molar conductivity at infinite dilution	126.45
B_0	Constant	0.3277
B_1	Constant	0.2271
B_2	Constant	54.164
u	Constant	4

Table 5.2: EDR Subsystem Parameters

Parameter	Description	Value
$Cost_{EDR}$	Cost of EDR cell pairs	\$50/cell pair
$Cost_{batt}$	Cost of batteries	\$350/kWh
$Cost_{PV}$	Cost of PV solar panels	\$162/m^2
RF_{EDR}	Replacement frequency of EDR membranes	1/lifetime
RF_{batt}	Replacement frequency of batteries	4/lifetime
RF_{PV}	Replacement frequency of solar panels	0/lifetime

Table 5.3: Cost and Replacement Frequency Parameters

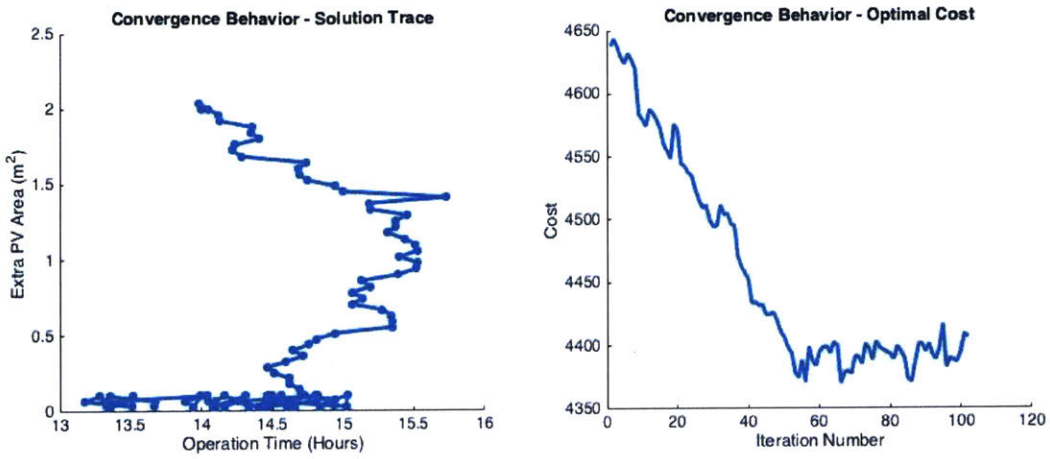

(a) The trace of steepest descent in the design space.

(b) Cost convergence of the steepest descent trace.

Figure 5-4: Steepest descent solution traces.

Constraints

The constraints on the optimization problem are the following:

$$0 \leq t_{op} \leq 24 \tag{5.10}$$

$$A_{PV,extra} \geq 0 \tag{5.11}$$

The first constraint represents the requirement that daily operating time must fall within the bounds of a day, and the second constraint ensures that the area of PV panels for the design is at least enough to provide the energy needed for desalination.

5.2.3 Single-Objective Optimization Algorithms

Based on this problem formulation, an ensemble of gradient-based and heuristic optimization algorithms was used to obtain a better-optimized design than what could be obtained by using either algorithms independently.

Gradient-Based: Steepest Descent

Steepest descent [32] was chosen as a representative of gradient-based optimization algorithms. The gradient was numerically approximated using a central difference approach that requires (n+1) model evaluations in each iteration of the algorithm, where n is the number of decision variables. A full factorial [31] design of experiments approach was used to determine the initial starting point of the algorithm. The algorithm converged initially to a point with a high condition number. A hessian-based scaling [32] showed that the decision variable t_{op} needed to be scaled down one order of magnitude. Tuning the step size parameter α of the steepest descent algorithm helped the algorithm to avoid jumping into a sub-optimal solution. Figure 5-4a shows the trace that steepest descent took from the initial point suggested by the design of experiments to the optimal solution, while Figure 5-4b shows the performance (cost) of each corresponding iteration. The algorithm terminated by exceeding the number of allowed iterations. Generally, the algorithm works as follows: an approximation of the gradient is calculated through central difference, a proportion α of the negative of the gradient is then taken as a step from the current location, this process is iterated through until the algorithm terminates. Termination occurs when the change in objective value is smaller than a tolerance value, or when the number of the maximum allowed number of iterations is exceeded.

Heuristic Algorithms: Particle Swarm Optimization

In the class of heuristic-based optimization algorithms, particle swarm optimization (PSO) [27] was used. The algorithm is parametric, meaning that it is sensitive to parameter settings. The algorithm mimics the swarming behavior usually exhibited by some biological communities (i.e. birds, bees, etc..) where an individual member of the community mimics the behavior shown by others in the same community, leading to the emergence of a collective swarm-like behavior. The success of some biological communities in finding optimal sources of food is attributed to this swarming behavior. The algorithm functions by initiating a population of particles with spe-

cific characteristics: position, velocity, and fitness. The position of each member is updated based on velocity, and velocity, in turn, is updated based on the algorithm's parameters: an inertia factor, the current motion, the particle's self confidence, a particle's memory influence, a swarm confidence and a swarm influence [27]. The algorithm terminates when the change in the maximum fitness among the swarm is below a specified tolerance level, or the number of iterations exceeds a specified number. Using the PSO parameter settings summarized in Table 5.4 gave the best results.

Parameter	Description	Value
N	Swarm size	5
w	Inertia	0.5
c_1	Self confidence	1.5
c_2	Swarm confidence	1.5
e	Convergence criterion	50
s	Convergence steps	10
d_t	Time step	10

Table 5.4: PSO Tuning Parameters

5.2.4 Multi-Objective Optimization

In the multi-objective optimization, the recurring cost J_2 is considered along with capital cost. Similar to the adaptive weighted sum method, the manual weighted sum method uses the following objective function:

$$J = \lambda J_1 + (1 - \lambda) J_2 \tag{5.12}$$

where λ is the weighting factor between J_1 and J_2. By considering values 0.00, 0.01, 0.02, 0.03, ... , 1.00, a detailed Pareto front was generated. As a comparison method, a full factorial study was run.

5.3 Results and Discussion

5.3.1 Single-Objective Optimization Results

The results of the two single-objective optimization algorithms are summarized in Table 5.5. Both methods converge on very similar designs, with PSO arriving at a slightly lower capital cost. For the parameters used here, extra PV area decreases battery requirements but increases overall cost, so the optimal solution has approximately no extra PV area. This implies that the constraint on PV area is active, suggesting that reductions in the energy requirement for EDR would allow the total system cost to be reduced even further.

	Steepest Descent	**Particle Swarm Optimization**
Capital Cost	\$4,370	\$4,360
t_{op}	15.02 h	15.83 h
$A_{PV,extra}$	0.03 m^2	0.00 m^2
$E_{battcap}$	3.09 kWh	3.33 kWh

Table 5.5: Comparison of optimal solutions obtained by steepest descent and PSO.

5.3.2 Multiple-Objective Optimization Results

The design space and Pareto fronts generated by the manual weighted sum and full factorial studies are illustrated in Figure 5-5.

These results show fair agreement, although the manual weighted sum method was unable to capture the same optima demonstrated by the full factorial study near the high values of J_1 and low values of J_2. This was likely due to a limitation of MATLAB function *fmincon* to adequately optimize the problem using our models.

5.3.3 Sensitivity Analysis

Running a sensitivity analysis around the optimal solution on the model parameters shows that an increase in feed salinity results in an increase in cost. Similarly, a decrease in solar irradiance also causes an increase in cost, as shown in Figure 5-6. This intuitively makes sense, since higher salinities require a greater energy input

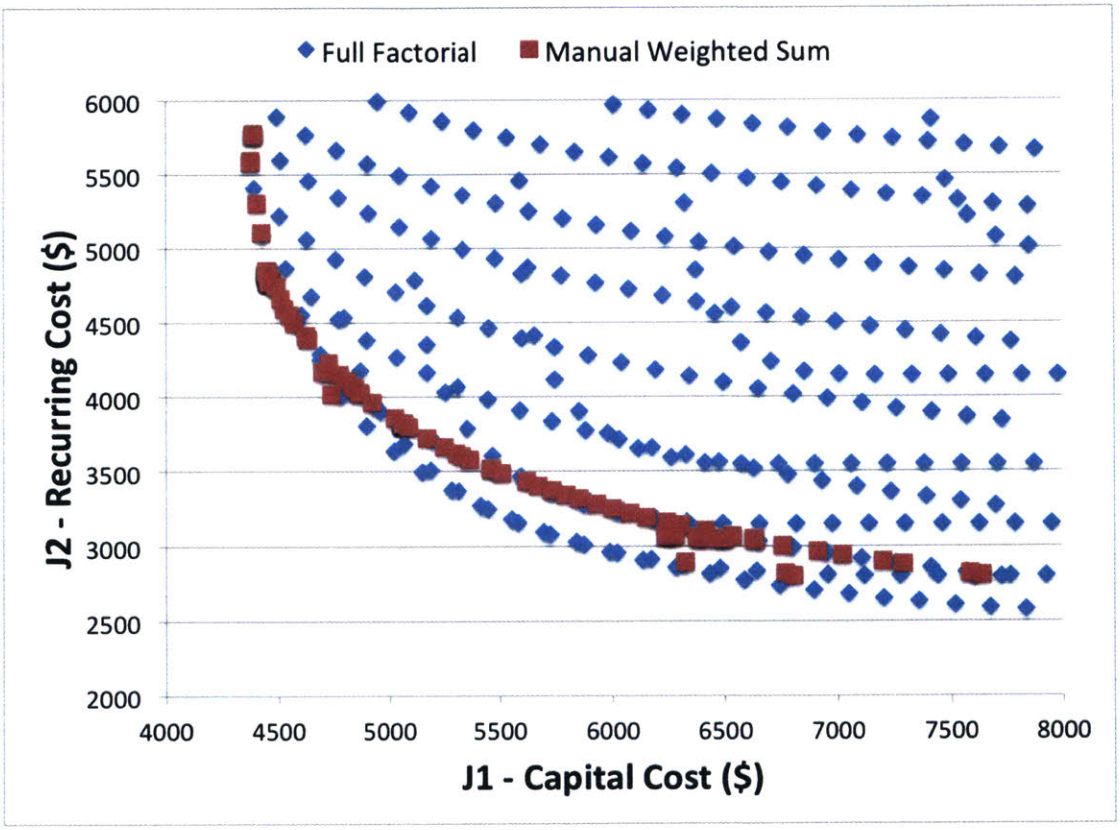

Figure 5-5: Pareto front generated by the manual weighted sum.

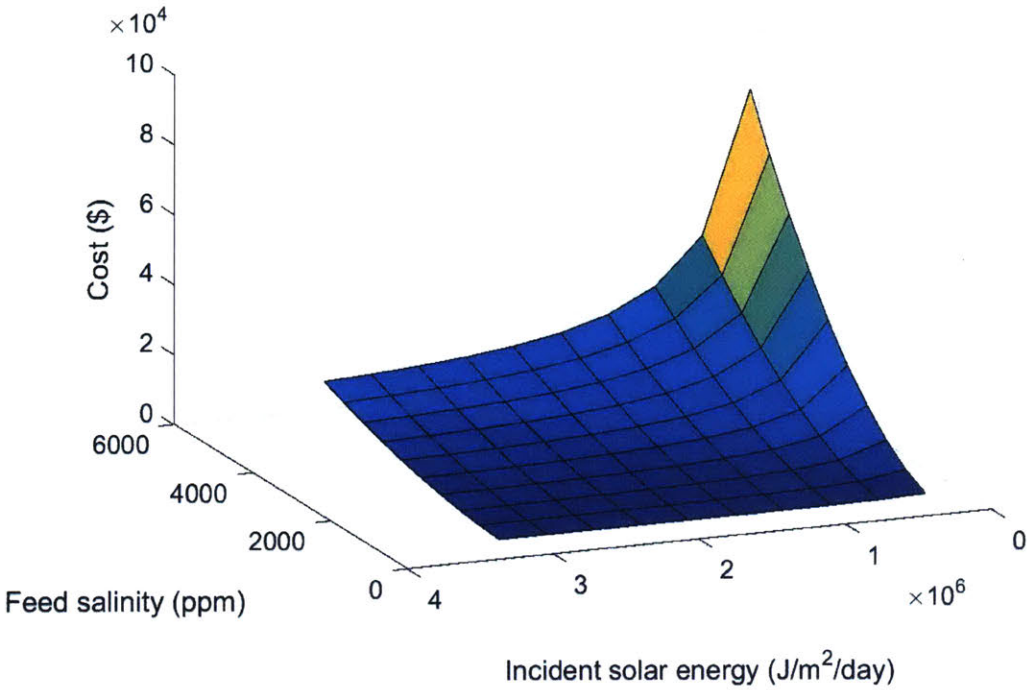

Figure 5-6: Sensitivity analysis of the PV-EDR system to changes in intake salinity and solar irradiance around the optimal solution.

to produce potable water, resulting in higher PV power system costs. Similarly, low solar irradiance requires more solar panels to generate the necessary amount of energy to run the EDR system.

5.4 Conclusion

In this chapter, the results of two methods for optimizing a PV-powered EDR desalination system have been presented. The optimal combinations of PV panels, batteries, and EDR cell pairs at which the system capital cost and 20-year recurring cost are minimized were found and compared. The capital cost and 20-year recurring cost functions were minimized using single-objective steepest descent and particle swarm optimization algorithms. A multi-objective full-factorial experiment and manual weighted sum were conducted to generate a Pareto front comparing the capital cost and 20-year recurring cost.

Site specific parameters would reveal sensitivity to capital costs and recurring costs. This information would inform the ideal weighted preferences and thus the full system design and pricing. Future extensions of this work may include an expansion of the design variables to consider additional EDR parameters, such as the linear velocity of the fluid flow. Additionally, a water tank for buffering solar irradiance day-to-day variations may be included as a design variable, as the analysis is expanded to look at the entire annual solar radiation cycle. The cost model will be expanded in future work to include other components, such as pumps, charge controllers, and structural materials. An additional extension of this research will be further sensitivity analyses of component costs, such as the ratio of battery to PV cost and its impact on component quantities and operating time.

Bibliography

[1] Preliminary Results of the 2010 Census, Central Department of Statistics and Information (CDSI), Riyadh, Saudi Arabia, 2010

[2] Annual Report, Ministry of Water and Electricity (MoWE), Riyadh, Saudi Arabia, 2014

[3] Multsch, S., Alrumaikhani, Y.A., Alharbi, O.A., Frede, H.-G., Breuer, L. 2011 "Internal water footprint assessment of Saudi Arabia using the Water footprint Assessment Framework (WAF)" 19th International Congress on Modelling and Simulation, Perth, Australia, 12âĂŞ16 December 2011

[4] H. M. H. Al-sheikh, âĂIJCountry Case Study - Water Policy Reform in Saudi ArabiaâĂİ in The second expert consultation on national water policy reform, 1997, pp. 1âĂŞ20.

[5] Groundwater Management in Saudi Arabia, Food and Agriculture Organization of the United Nations, Rome, Italy, 2009

[6] Morris, B L, Lawrence, A R L, Chilton, P J C, Adams, B, Calow R C and Klinck, B A. (2003) Groundwater and its Susceptibility to Degradation: A Global Assessment of the Problem and Options for Management. Early Warning and Assessment Report Series, RS. 03-3. United Nations Environment Programme, Nairobi, Kenya.

[7] World Population Prospects: The 2012 Revision, United Nations Department of Economic and Social Affairs

[8] Midyear Population estimates: Regional Level for 2010-2025, Central Department of Statistics and Information (CDSI), Riyadh, Saudi Arabia, 2010

[9] Water Resources System, Ministry of Water and Electricity (MoWE), Riyadh, Saudi Arabia, Available: http://app.mowe.gov.sa/ipspublic/

[10] Annual Statistics Book, Saudi Arabian Monetory Agency (SAMA), Riyadh, Saudi Arabia, 2013

[11] Ninth Development Plan: Chapter 28: Agriculture, Ministry of Economy and Planning, Riyadh, Saudi Arabia, 2010

[12] The Labor Force Survey, General Authority for statistics (GAStat), Riyadh, Saudi Arabia, 2013

[13] Ishimatsu, T. (2013). Generalized Multi-Commodity Network Flows: Case Studies in Space Logistics and Complex Infrastructure Systems. PhD Thesis. Massachusetts Institute of Technology. Cambridge, MA, USA.

[14] Ishimatsu, T., Doufene, A., Alawad, A., and de Weck, O.L. (2015a). "Desalination Network Model Driven Decision Support System: A Case Study of Saudi Arabia." IDA World Congress 2015, San Diego, CA.

[15] A.Doufen, T. Ishimatsu, A. Alhassan O. de Weck, K. Strzepek, A. Alsaati. 2015 "Large Scale Engineering Systems - Insight on Desalination for Agriculture in Saudi Arabia". The 26th Annual International symposium of the International Council on Systems Engineering. 2016

[16] S. Multsch, Y. A. Al-Rumaikhani, H.-G. Frede, L. Breuer. 2013 "A Site-sPecific Agricultural water Requirement and footprint Estimator (SPARE:WATER 1.0)". Geosci. Model Dev., 6, 1043âĂŞ1059, 2013

[17] Stefan Siebert, Verena Henrich, Karen Frenken and Jacob Burke (2013). Global Map of Irrigation Areas version 5. Rheinische Friedrich-Wilhelms-University,

Bonn, Germany / Food and Agriculture Organization of the United Nations, Rome, Italy

[18] Kingdom of Saudi Arabia Imports, General Authority for statistics (GAStat), Riyadh, Saudi Arabia, 2015

[19] Power Consumption Tariffs, The Saudi Electricity Company. https://www.se.com.sa/en-us/customers/Pages/TariffRates.aspx

[20] 2016 Annual Report, Ministry of Environment, Water and Agriculture. Riyadh, Saudi Arabia

[21] WHO / UNICEF Joint Monitoring Programme. âĂIJImproved and unimproved water sources and sanitation facilities,âĂİ Available at: http://www.wssinfo.org/definitions-methods/watsan-categories/. (Accessed: 2016).

[22] World Bank. "Access to electricity (% of population)". http://data.worldbank.org/indicator/EG.ELC.ACCS.ZS. (Accessed 2016).

[23] Bian, D. (2016, January). Personal interview.

[24] K. Bourouni, T. Ben MâĂŹBarek, A. Al Taee, âĂIJDesign and optimization of desalination reverse osmosis plants driven by renewable energies using genetic algorithms,âĂİ Renewable Energy 936-950, 36 (2011)

[25] J. Kim et al., âĂIJDesign optimization of a solar-powered reverse osmosis desalination system for small communities,âĂİ IDETC/CIE (2013)

[26] E. Koutroulis, D. Kolokotsa, âĂIJDesign optimization of desalination systems power-supplied by PV and W/G energy sources,âĂİ Desalination 171-181, 258 (2010)

[27] J. Kennedy and R. Eberhart, "Particle swarm optimization," Neural Networks, 1995. Proceedings., IEEE International Conference on, Perth, WA, 1995, pp. 1942-1948 vol.4. doi: 10.1109/ICNN.1995.488968

[28] Wright, N. (2014). "Justication of Village Scale Photovoltaic Powered Electrodialysis Desalination Systems for Rural India" Master's thesis, Massachusetts Institute of Technology, Cambridge, Massachusetts.

[29] H. Strathmann. Assessment of electrodialysis water desalination process costs. In Proceedings of the International Conference on Desalination Costing, Limassol, Cyprus, 2004.

[30] M. Ortiz, J.a. Sotoca, E. Exposito, F. Gallud, V. Garca-Garca, V. Montiel, and a. Aldaz. Brackish water desalination by electrodialysis: batch recirculation operation modeling. Journal of Membrane Science, 252:65-75, 2005.

[31] Ronald Fisher (1926). "The Arrangement of Field Experiments" (PDF). Journal of the Ministry of Agriculture of Great Britain 33: 503âĂŞ513.

[32] Meza, J. C. (2010). Steepest descent. Wiley Interdisciplinary Reviews: Computational Statistics, 2(6), 719-722. Chicago